May 2008

Superpave In Situ Stress/Strain Investigation – Phase II
(SISSI II)

# Draft Report:

# Independent Mechanistic Analysis using SISSI Dynamic Data

## Introduction

The effectiveness of any mechanistic-based pavement design depends on the accuracy of employed mechanistic parameters, such as stress and strain. There are three common approaches that can be used to compute the stresses and strains in pavement structures: layered elastic analysis, two-dimensional (2-D) finite element (FE) modeling, and three-dimensional (3-D) finite element modeling.

Layered elastic analysis (LEA) has been widely used to solve pavement engineering problems, in which each layer is treated as a horizontally continuous, isotropic, homogenous, and elastic medium. Elastic modulus and Poisson's ratio are important in controlling material behavior. A uniformly distributed vertical tire pressure around a circular or rectangular area is assumed. The thickness of each individual layer and material properties may vary from one layer to the next. However, continuity conditions at the interface are satisfied1. In other words, the two adjacent layers have the same level of vertical stress, deflection, shear stress, and radial displacement. Several programs such as KENLAYER (Huang 1993) and BISAR (De Jong et al. 1973) calculate stresses and strains in pavement structures using this type of analysis. Although theoretical calculations using the layered theory are relatively inexpensive and easy, typical assumptions, such as that materials must be homogenous and linearly elastic within each layer and that the wheel loads applied on the surface must be axis-symmetric, significantly affect the reliability of analysis results. This effect becomes more pronounced when predicting pavement response under complex loading and environmental conditions. Hence, a more advanced theoretical analysis tool, such as the FE method, would be needed.

The limitations of layered elastic analysis are the strengths of finite element analysis. In theory, the FE method allows a system to be analyzed as an assemblage of discrete bodies referred to as finite elements, and approximate solutions of governing partial differential equations are developed to describe the response at specific locations on each body, called nodes or nodal points. Complete system responses are computed by assembling individual element responses while satisfying continuity at the interconnected boundaries of each element. The FE method is by far the most universally applied numerical technique for flexible pavements (MEPDG 2004). It provides a modeling alternative that is well suited for applications involving pavement systems with inelastic materials, unusual boundary constraints, or complex loading conditions. Generally, the computational time for LEA increases with number of layers and with number of required stress computation points (e.g., to determine the critical locations for the critical response parameters and for superposition of multi-wheel loading cases). In contrast, an FE solution (assuming a sufficiently fine mesh) will not require significant additional computation time as the number of layers and/or stress computation points increases. The FE meshing already divides the pavement structure into many thin layers (theoretically, each layer of elements in the mesh could be assigned properties corresponding to different pavement layers), and the FE algorithms automatically determine the stresses and strains at all element integration points.

In 2-D FE modeling, plane strain or axis-symmetric conditions are generally assumed. Compared to the layered elastic analysis, the practical applications of 2-D FE modeling are greater because they can rigorously handle material anisotropy, material nonlinearity, and a variety of boundary conditions. Unfortunately, 2-D FE models cannot accurately capture spatial response under multiple wheel loads. Discrete vertical discontinuities are important three-dimensional geometric features in some flexible and composite pavement rehabilitation scenarios, in particular with regard to reflection cracking, which was not considered in this study. To overcome the limitations inherent in 2-D FE modeling approaches, 3-D FE models have gained increasing attention. However, computational cost and time increase with 3-D models as model dimensions, material properties, and mesh generation become more complicated.

## Analysis of Pavement Temperature

One of the most important aspects of temperature data analysis is the variability of pavement temperature with depth because of its impact on accurate computation of flexible pavement response. In flexible pavements, layer moduli are significantly affected by the pavement temperature because the stiffness of the AC materials dramatically influences the structural capacity of flexible pavement. As the pavement temperature increases, its stiffness decreases, leaving it less able to withstand wheel load. A decrease in the stiffness results in higher stress being transmitted to the base and subgrade. In the following sections, detailed analyses of pavement temperature profiles are presented.

## Pavement Temperature at Blair

Two typical pavement temperature profiles are plotted in Figure 1 for spring and fall, respectively. Both profiles suggest that temperatures in the upper layers vary significantly as compared to the underlying layers, especially during spring. A complete summary of pavement temperatures at mid-depth of each AC layer during dynamic data measurements is provided in Table 1. These measured temperatures were selected to validate 3-D FE modeling, which will be discussed later in this report. In the analysis of pavement temperature, the mid-depth temperature of each AC layer was approximated from the temperatures above and below using a simple linear interpolation.

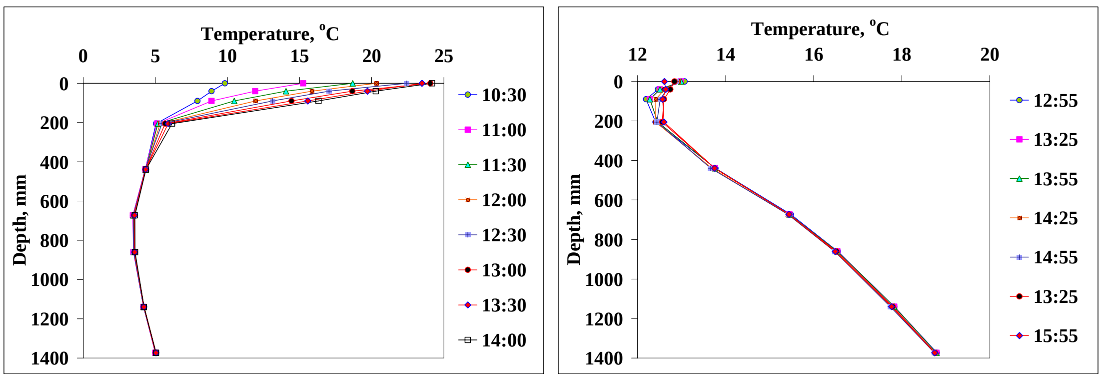


(a) Spring (b) Fall

**Figure 1. Measured temperature during dynamic data collections at Blair**

**Table 1. Measured temperatures during dynamic data collections at Blair.**

| Date | Time | Pavement Temperature @ mid-depth, °C | | |
|---|---|---|---|---|
| | | Wearing | Binder | BCBC |
| 5/4/2004 | 13:36 | 31 | 28 | 18 |
| 7/20/2004 | 10:32 | 31 | 28 | 26 |
| 7/20/2004 | 12:25 | 31 | 28 | 26 |
| 10/21/2004 | 14:35 | 13 | 13 | 12 |
| 10/21/2004 | 15:06 | 13 | 13 | 12 |
| 3/7/2005 | 11:22 | 16 | 12 | 5 |
| 3/7/2005 | 11:33 | 16 | 12 | 5 |
| 3/7/2005 | 11:58 | 17 | 14 | 5 |
| 3/7/2005 | 12:57 | 20 | 17 | 6 |
| 3/7/2005 | 13:30 | 21 | 18 | 6 |
| 3/7/2005 | 13:42 | 21 | 18 | 6 |
| 8/23/2005 | 11:32 | 35 | 33 | 29 |
| 8/23/2005 | 11:49 | 37 | 33 | 29 |

## Pavement Temperatures at Warren

At Warren, thermocouples were placed only at the bottom of the wearing and leveling layers during field instrumentation. Thus, the mid-depth temperatures cannot be linearly interpolated from measured temperatures. When measured pavement temperatures are not available, a common practice is to predict temperatures using prediction models. Several models have been developed and are available. Some of these models are in use in North America and internationally, such as the AASHTO and the Asphalt Institute models, while others were developed through research efforts specifically for certain regions or states. The following sections review some of the existing models and research in this domain. Pavement temperatures predicted from a selected model are presented at the end.

## Review of Temperature Prediction Models

The 1993 AASHTO guide provides standards and guidelines that are mainly used in the design and restoration of flexible, rigid, and composite pavements. AASHTO recommends either directly measuring the AC mix temperature or estimating it from surface and air temperatures. AASHTO recommends, as a minimum, determining the temperature at the top, middle, and bottom of the AC layer and using the average of these temperatures to represent the temperature of the AC layer. However, the predictions were developed based on data collected from a limited number of sites.

The Asphalt Institute developed a prediction model to accurately estimate the AC temperature at various depths. This model was based on having the sum of the surface temperature and average air temperature for five days prior to testing day as an input for the model. Even though this approach is widely used across the United States, the applicability of these models to all regions is questionable because these models were developed at certain locations and under certain environmental conditions, which might not be consistent across the nation.

The Federal Highway Administration Long Term Pavement Performance (LTPP) program is another well-known research program in North America. The results of analyses performed on data collected under the LTPP program is intended to improve the pavement performance and increase pavement service life. In 2000, Lukanen et al. carried out a study to investigate the effects of temperature on AC pavement deflections using the data collected under the Seasonal Monitoring Program (SMP) of the LTPP program. The objectives of this study were to develop a model that could be used to predict the temperature within an AC layer from surface temperature data collected during routine deflection testing and to develop relationships between AC temperature, pavement deflections, and backcalculated AC modulus. A series of improvements was introduced in this study to the well-known BELLS model in an attempt to develop an enhanced temperature prediction model within AC pavement (Lukanen et al. 2000). The original BELLS model predicts mid-depth AC layer temperature using the AC layer thickness, 5-day mean air temperature, infrared surface temperature reading, and time of day. It was found that due to faulty infrared surface temperature probes used during data collection, the original BELLS model is only valid for a temperature range of 15-25°C. It over-predicts the AC temperature at lower temperatures and under-predicts it at higher temperatures. Therefore, a second model, BELLS2, was developed using corrected infrared surface temperature data and an expanded database. In this model, the average of the previous day's high and low air temperatures was used instead of the 5-day mean air temperature, thus reducing the amount of data required to make use of the model. When the data used to develop BELLS2 was further investigated, it was found that, as per LTPP data collection protocol, the pavement surface was shaded for an average of six minutes prior to temperature sampling. Therefore, a third model, BELLS3, was developed for use during routine FWD testing, when the pavement surface is typically shaded for less than a minute. A semi-logarithmic format equation relating the AC modulus to the mid-depth AC temperature was developed to allow for a simple means of adjusting the backcalculated AC modulus for the effects of temperature. Even though BELLS3 has introduced some improvements to the original BELLS model, it has some limitations that might hinder its normalization (Marshall et al. 2001). The BELLS models are based on daytime surface temperature data collected at above-freezing temperatures, so their use during nighttime hours and at below-freezing temperatures may be problematic. In addition, these equations should only be used for AC layer thicknesses of 45 mm-305 mm, which is the range contained in the LTPP database.

In an attempt to investigate the impact of moisture content and other environmental parameters on pavement strength, an Integrated Climatic Model (ICM) was developed by Lytton et al. (1990). ICM was further enhanced in 1997 (EICM) by Larson and Dempsey. EICM has the capability of generating patterns of rainfall, solar radiation, cloud cover, wind speed, and air temperature to simulate the upper boundary conditions of a pavement soil system. The program calculates the temperature, suction, and pore pressure without loading effects, moisture content, and resilient modulus for each node in the profile for the entire analysis period, as well as frost, infiltration, and drainage behavior. The input to EICM includes data such as latitude, geographic region, and number of days in analysis period, as well as background information on the thermal properties associated with the site of interest. The surface temperature is initially established and is followed by the calculation of temperatures throughout the pavement layers. Once the surface temperatures are determined, they are used to calculate the temperature throughout the underlying pavement layers. A one-dimensional heat transfer model is used to determine the distribution of temperatures in the pavement layers. In a study conducted by Birgisson et al. (2000), using the EICM, it was reported that AC stiffness is responsive to temperature. Accordingly, when the EICM was tested for the changes in stiffness of the pavement materials under the influence of changing temperature, it was found that trends in the predicted temperatures in the AC layer compared very favorably with those observed in the field. As a model input, EICM requires the analysis parameters (exact date and duration of the analysis period at the location), specific climatic data (minimum and maximum daily air temperature, rainfall, wind speed, percent sunshine, and water table depth for the each day in the analysis period), pavement material properties (thermal properties, infiltration, and drainage properties), pavement structure (layer material and thickness), and subgrade properties.

Considering that EICM has been fully included in the MEPDG for pavement performance predictions, it is reasonable to use EICM to predict pavement temperature so that the overall research consistency is maintained. Consequently, a stand-alone version 3.2 of EICM was used in this study to predict pavement temperatures at Warren.

## Predicting Warren Pavement Temperatures Using EICM

The EICM program user has a choice of using either the Hourly Climatic Database supplied with the EICM or actual field-specific data (if available). Since some of the actual field-specific data, such as percent sunshine and subgrade properties, were not complete, hourly climatic data from weather stations close to Warren were input into the EICM. Two pavement temperature profiles predicted from the EICM are plotted in Figure 2 for summer and winter, respectively. These figures suggest that EICM-predicted temperature profiles compare marginally with the actual measured temperature profiles. A larger difference was found at both locations (bottom of wearing and leveling layers) although the difference between the measured and predicted temperatures became relatively small in the ground for the cold season. The comparison results match the findings obtained by other researchers (Heydinger 2003, Ahmad et al. 2005, Liang et al. 2006, and Zaghloul et al. 2006). These studies found a low correlation between the EICM-predicted temperature profiles for the various pavement layers when compared to the measured values. Therefore, it was decided to adjust temperature profiles from EICM based upon measured temperatures first. Then, mid-depth temperatures were further linearly interpolated from adjusted temperature profiles. This procedure is also demonstrated in Figure 2. A complete summary of pavement temperatures during dynamic data measurements at Warren is provided in Table 2. These measured temperatures were selected to validate 3-D FE modeling, which will be discussed in the next chapter.

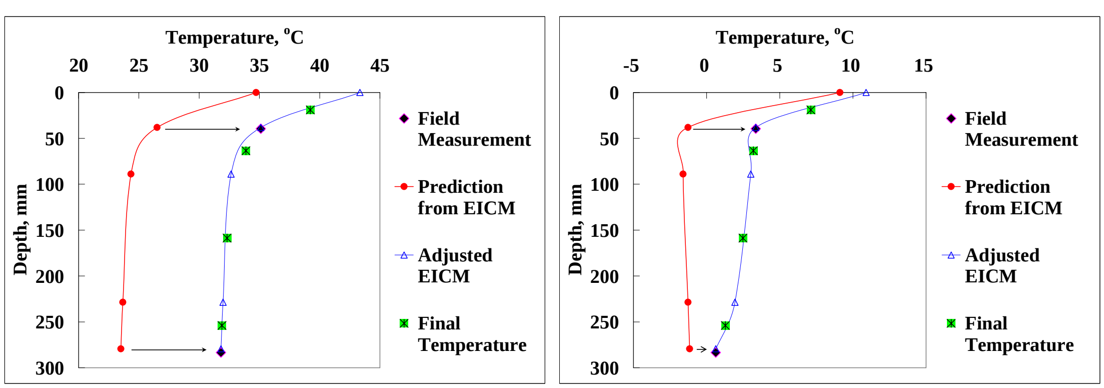

(a) Summer (b) Winter

**Figure 2. Adjusted pavement temperature profile at Warren**

**Table 2. Adjusted temperatures during dynamic data collections at Warren.**

| Date | Time | Pavement Temperature @ mid-depth, $^{o}$C | | | |
|---|---|---|---|---|---|
| | | Wearing | Binder | BCBC | Leveling |
| 6/27/2003 | 14:00 | 39 | 34 | 32 | 32 |
| 6/27/2003 | 14:21 | 41 | 35 | 34 | 33 |
| 6/27/2003 | 14:29 | 41 | 35 | 34 | 33 |
| 8/24/2004 | 10:33 | 31 | 24 | 22 | 22 |
| 8/24/2004 | 10:57 | 32 | 25 | 23 | 23 |
| 8/24/2004 | 11:10 | 32 | 25 | 23 | 23 |
| 8/24/2004 | 11:56 | 38 | 29 | 27 | 27 |
| 8/24/2004 | 12:12 | 38 | 29 | 27 | 27 |
| 8/24/2004 | 12:30 | 40 | 31 | 28 | 28 |
| 11/5/2004 | 13:06 | 11 | 9 | 8 | 8 |
| 11/5/2004 | 14:12 | 12 | 11 | 11 | 10 |
| 11/5/2004 | 14:31 | 13 | 11 | 11 | 10 |
| 11/5/2004 | 14:54 | 12 | 12 | 10 | 9 |
| 11/5/2004 | 14:56 | 12 | 12 | 10 | 9 |
| 11/5/2004 | 15:06 | 12 | 12 | 10 | 9 |
| 11/5/2004 | 15:16 | 12 | 12 | 10 | 9 |
| 3/17/2005 | 9:52 | 7 | 3 | 2 | 1 |
| 3/17/2005 | 10:05 | 7 | 3 | 2 | 1 |
| 3/17/2005 | 10:32 | 10 | 5 | 4 | 3 |
| 3/17/2005 | 11:05 | 11 | 8 | 7 | 5 |
| 3/17/2005 | 11:10 | 11 | 8 | 7 | 5 |
| 3/17/2005 | 11:29 | 14 | 9 | 7 | 6 |

## Simulation of Pavement Response

Finite element analysis is a general tool for solving structural mechanics problems, with its earliest application to civil engineering problems dating back to the 1960s. The basic concept of FEA is the subdivision of a problem into a set of discrete or finite elements. The geometry of each finite element is defined in the simplest case by the coordinates of the corners; these points are called nodes. The variation of displacements within an element is then approximated in terms of the displacements of the nodes and a set of interpolation functions. Bilinear interpolation functions are the simplest for rectangular elements. Equation 1 gives the relationship between element nodal displacements and strains:

$$E = SU \tag{1}$$

where $E$ is the strain vector, $S$ is a suitable linear operator, and $U$ is the nodal displacement vector. The element stiffness matrices are computed using:

$$K^e = \int B^T DBdv \tag{2}$$

where $B$ is a matrix of linear operators (derivatives of shape functions), and $D$ is the constitutive matrix. The element stiffness matrices are assembled for all elements, the boundary conditions are introduced, and the resulting equations are solved for incremental displacements, strains, and stresses. These are accumulated over the load increments to give the total displacements, strains, and stresses as functions of load level. An implicit FE formulation was used in this study, which means the loading is divided into relatively coarse increments, and an iterative technique is employed at the end of each increment to bring the internal stresses into equilibrium with the external applied loads.

The FE method is well suited for analyzing pavement engineering problems involving material nonlinearities and complex loading conditions. Such analysis proceeds by defining the characteristics of each pavement layer. The capabilities of the 3-D FE method for flexible pavement structural analysis are already well established in the literature (Zaghoul and White 1993, Chen et al. 1995, Cho et al. 1996, Hjelmstad et al. 1997, Shoukry 1998a, Uddin 1998, and White 1998).

The general purpose finite element software ABAQUS (version 6.6) was used in this study because of its capability in reducing the computation time through the use of 3-D reduced integration elements. ABAQUS also includes various material models, such as linear elastic, viscoelastic, and elastoplastic models. The following sections highlight some features of the developed FE model. A detailed validation study using field measurements and LVE solutions is also presented.

## Finite Element Modeling Strategy

Critical stresses and strains (peak values) typically tend to occur around the loads, and those should decrease in the far field. In FE modeling, there are two options for increasing the accuracy of results in the region of interest: 1) re-analyze the region of interest with greater mesh refinement or 2) generate an independent, more finely meshed model of only the region of interest, and analyze it. The first option can be time consuming and costly; therefore, the second option was further considered. After comparing several possible approaches, a Global-Local (G-L) hierarchical FE modeling approach was adopted. This approach has several advantages over traditional FE modeling techniques. First, it is a realistic 3-D FE model and can accurately calculate the spatial pavement response to loading. Second, it is capable of handling variable materials such as AC. Finally, through the cut-boundary displacement method, also known as the specified boundary displacement method (ABAQUS 2002), the developed FE model is made very efficient in terms of computing and hardware requirements. It enables users to experiment with different designs (e.g., finer mesh and quasi-static analysis procedure) for the region of interest.

In the first stage (global level) of the G-L approach, the pavement section subjected to loading and boundary conditions was analyzed using a relatively coarse mesh. In the second stage (local level), a more refined mesh was used to model a local part of the pavement section based on interpolation of the solution from the initial, relatively coarse, global model. The size of the local model depends upon the analysis objective and also upon the moving load simulated. The same types of elements as those in the global model analysis were used to mesh the local model. A very fine mesh was applied to the area of interest and to some depth under the pavement surface. The results of the global model were interpolated on the cutting edge of the local model corresponding to different calculation steps, and the interpolation results were applied as boundary conditions to the local model. The interpolated results from the global model solution at the nodes of the local model boundary are known as “driven variables” and define the degrees of freedom at these nodes. The advantage of running FE models in this fashion is that it allows for a convenient way to transfer the results of the global model to the local model. This greatly simplifies the process of simulating almost any area of interest by having to run the global model only once.

Due to symmetry in the transverse direction, only half width of the truck axle (915 mm) needs to be modeled if an assumption of equal wheel weight is satisfied. Two examples of a comparison of left and right wheel weights are shown in Figure 3. For both Blair and Warren, relatively high $R^2$ values suggest that it is reasonable to believe the axle weight is evenly distributed to the left and right wheels for these two specific SISSI sites. In the vertical direction, the thickness of the global model was predetermined by the pavement structure (3000 mm). In the longitudinal direction, the finite domain from the infinitely long AC pavement must be properly selected to deliver accurate predictions for stresses and strains in the field. The determination of the model's longitudinal dimension (traffic direction) is discussed later in this section.

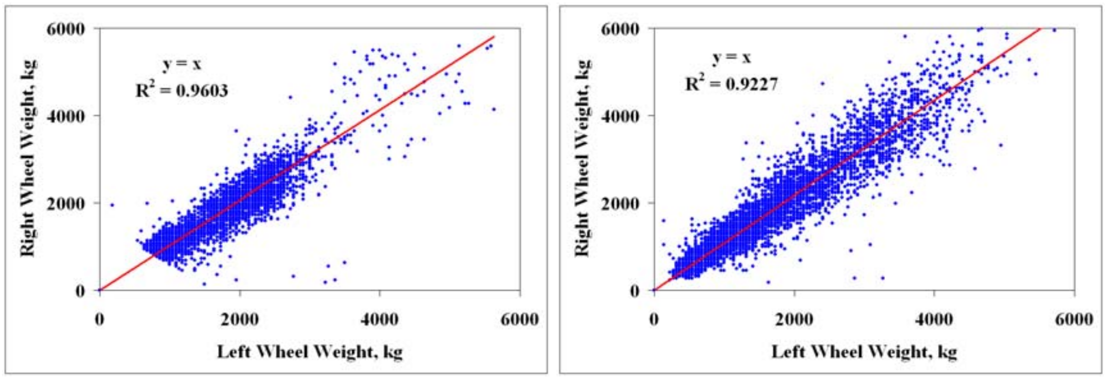


(a) Warren (b) Blair

**Figure 3. Comparison of left and right wheel weights.**

**Boundary Conditions**

Generally, pavements and their supporting structures are modeled as infinite media in longitudinal and transverse directions; how the unbounded domain is treated is an important issue in FE modeling of pavements. In FE modeling, boundary conditions are usually represented by mathematical models. The mathematical model for the Blair pavement structure is shown in Figure 4. The bottom of the model was prevented from axial movements in the three directions to represent the bedrock (rigid layer) beneath the pavement structure. Kuo et al. (1995) and Zaghloul and White (1993) have successfully adopted such boundary conditions. All the sides of the model were also fixed in all directions except the one at the centerline of the truck axle. This symmetry line was fixed in the *y* direction, which is perpendicular to the longitudinal direction. This boundary condition setting usually increases the stiffness of the pavement structure and leads to smaller calculated displacements than actual values, especially for points near the truncated boundaries. However, the error due to the boundary effects would be negligible if the model dimensions were chosen to be appropriate. All layers were considered perfectly bonded to one another so that the nodes at the interface of two layers had the same displacement in all three (*x*, *y*, and *z*) directions. This bonding treatment probably represents the interface condition for hot-mix asphalt (HMA) layers more closely than the subbase/subgrade interface, where possibility of slippage is more dominant. These boundary conditions are applicable to the FE models for both Blair and Warren.

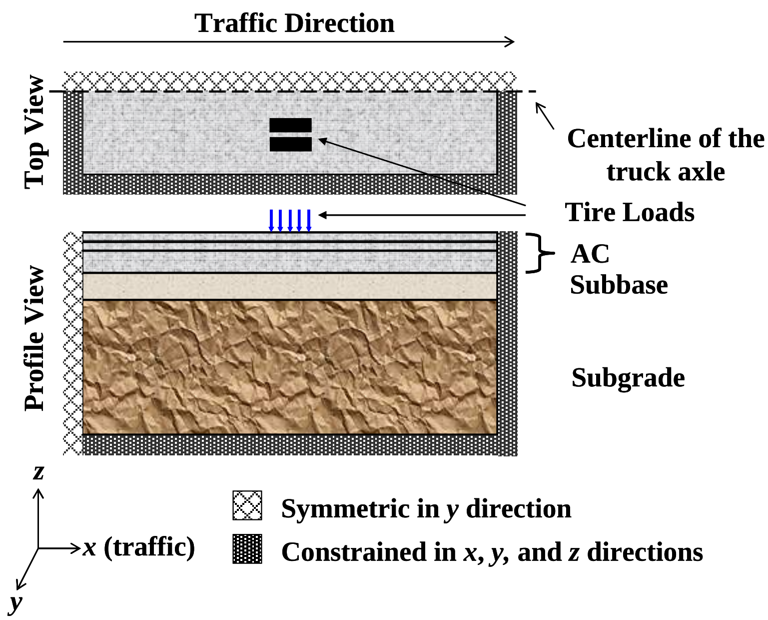


**Figure 4. Mathematical model representing the boundary conditions.**

## Material Properties

Among the most important parameters needed as input for mechanistic-empirical pavement design models are the properties of materials used in different pavement layers. In order to obtain properties, the materials were considered in two general categories: bound materials (AC) and unbound materials (fractured PCC at Warren, granular subbase, and subgrade). At high temperatures or under slow loading rates, AC mixtures exhibit a viscous flow, which results in load-associated distresses such as permanent deformation. On the other hand, at low temperatures or under fast cooling rates, an AC mixture becomes stiffer and more brittle, which makes it vulnerable to non-load-associated distresses such as thermal cracking. Fatigue cracking is a more dominant type of distress at intermediate temperatures because a significant part of the traffic load is applied at these temperatures. Granular materials are large conglomerations of discrete macroscopic particles. If they are non-cohesive, then the forces between particles are essentially only repulsive so that the shape of the material is determined by external boundaries and gravity. If they are dry, then any interstitial fluid, such as air, can be neglected in determining many of the flow and static properties. Granular materials typically exhibit a stress-dependent response. The materials become stiffer as higher stress is applied.

**Bound Materials**

Advances in computing power and material characterization methodologies have led to more sophisticated utilization of constitutive models to realistically predict viscoelastic materials' responses under different loading rates and temperatures. The viscoelastic behavior of AC materials can be represented by a Prony series expansion of the dimensionless shear and bulk relaxation modulus, which is a mathematical formulation for a mechanical analog of viscoelastic materials known as the Wiechert model. The Wiechert model is a parallel combination of sets of springs and dashpots connected in series to each other:

$$E(t) = E_\infty + \sum_{1}^{m} E_i e^{-\left(\frac{t}{\rho_i}\right)} \tag{3}$$

where $E_\infty$ is the long-time relaxation modulus (e.g., at an infinite loading time), $E_i$ are Prony coefficients, and $\rho_i$ are relaxation times that are explicit functions of the dashpot viscosities and corresponding spring stiffnesses. Theoretically, the coefficients $E_i$ can be obtained by assuming a set of $\rho_i$ at regular intervals of one decade (multiples of 10) or one-half decade (half multiples of 10). The advantage that the Prony series has over other viscoelasticity representations is the associated computational efficiency and simplicity. However, owing to experimental constraints such as limitations of machine loading capacity, the relaxation modulus test is rarely conducted in the laboratory. It is well accepted that all linear viscoelastic material functions are mathematically equivalent, and each function contains essentially the same information on the relaxation and creep properties of the material. As a result, a linear viscoelastic material function can be converted into other material functions through appropriate mathematical operations (e.g., from frequency domain to time domain). Consequently, a numerical method was used to obtain shear and bulk relaxation moduli indirectly from frequency-dependent test (complex modulus test) data. Shear and bulk relaxation moduli were computed from $|E^*|$ master curves, as proposed by Schapery and Park (1999):

$$\begin{aligned} G(t) &= \frac{|E^*|\cos\phi}{2\Gamma(1-n)\cos\left(\frac{n\pi}{2}\right)(1+\nu)} \\ K(t) &= \frac{|E^*|\cos\phi}{3\Gamma(1-n)\cos\left(\frac{n\pi}{2}\right)(1-2\nu)} \end{aligned} \tag{4}$$

where *G(t)* is shear relaxation modulus, *K(t)* is bulk relaxation modulus, $\phi$ is phase angle, $\Gamma$ denotes the gamma function, $\upsilon$ is Poisson's ratio, and $n$ is the slope of the $|E^*|$ master curve in log-log domain at each point in time. Relaxation moduli at time $t$ were also normalized by relaxation moduli at zero time. Shear relaxation modulus and bulk relaxation modulus master curves are plotted in Figures 5 and 6, respectively. At short times, the relaxation modulus is at a high plateau corresponding to the instantaneous response and then falls exponentially to the long-term response as the asphalt molecules gradually accommodate the strain by conformational extension rather than bonding distortion.

One important parameter in Equation 4 is Poisson's ratio. In the infinitesimal deformation of an idealized purely elastic compressible material, one may define a time-independent material constant, called Poisson's ratio, as the ratio of the lateral contraction to the elongation in an infinitesimally small uniaxial extension. In the infinitesimal deformation of any real material (e.g., viscoelastic), the lateral contraction is dependent on loading time or (as is equivalent) frequency. Obtaining the Poisson's ratio of viscoelastic materials is particularly challenging because it requires material testing under both normal and shear stress states under various temperatures and loading rates. Based on recommendations from the MEPDG (ERES 2004), a constant value of 0.30 was assumed for Poisson's ratio of AC mixtures. This magnitude for Poisson's ratio possibly results in smaller strains.

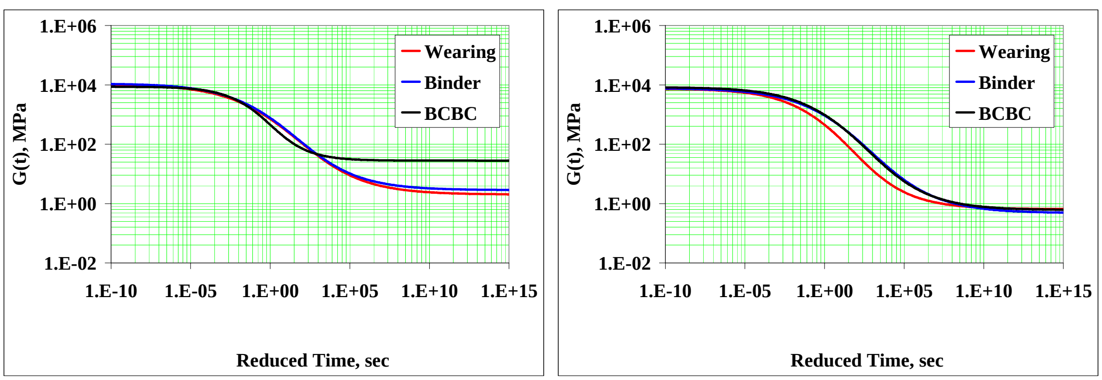


(a) Blair (b) Warren

**Figure 5. Shear relaxation modulus master curves.**

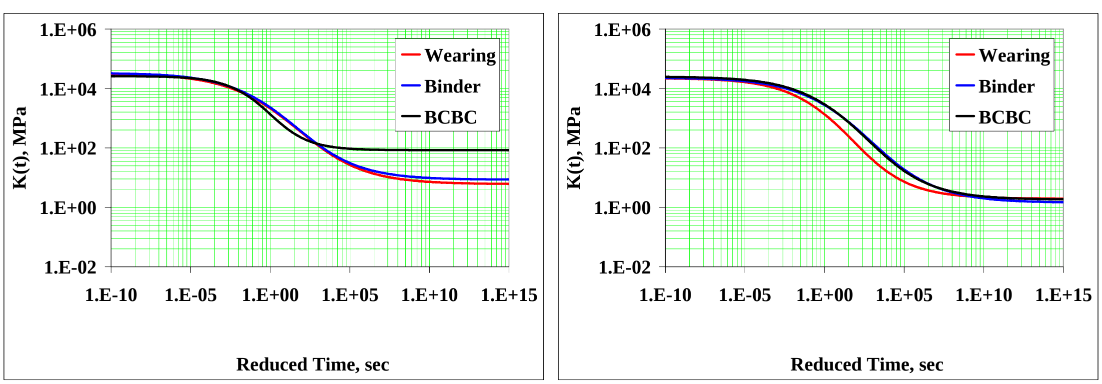


(a) Blair (b) Warren

**Figure 6. Bulk relaxation modulus master curves.**

## Unbound Materials

The properties of sublayer materials, such as fractured PCC, subbase and subgrade soils, are often not as well characterized as those of AC. In this study, this difficulty was overcome by backcalculating effective layer moduli from Falling Weight Deflectometer (FWD) data so that the FE model reasonably predicts the response of unbound materials. For the SISSI project, the FWD data analysis steps conducted were similar to those utilized for the LTPP data analysis. Backcalculated moduli considering seasonal effects are provided in Table 3 and Table 4 for Blair and Warren, respectively. These moduli were not varied with depth in the FE model.

**Table 3. Summary of backcalculated moduli for unbound materials for Blair**

| Season | Backcalculated Moduli, MPa | | Pavement Temperature, $^{o}C$ |
|---|---|---|---|
| | Subbase | Subgrade | |
| Spring | 418 | 106 | 4-5 |
| Summer | 27 | 209 | 23-25 |
| Fall | 681 | 114 | 7-8 |

**Table 4. Summary of backcalculated moduli for unbound materials for Warren**

| Season | Backcalculated Moduli, MPa | | Pavement Temperature, $^{o}C$ |
|---|---|---|---|
| | PCC | Subgrade | |
| Spring | 278 | 276 | (-3)-(-2) |
| Summer | 456 | 228 | 21-23 |
| Fall | 159 | 329 | 12-13 |

## Simulation of Moving Load

To accurately simulate pavement response to vehicular loading, the contact pressure distribution and dimensions of the contact area between the tire and pavement are required. In the layered theory, because of its use of axisymmetric solutions, the contact area is assumed to be circular although a rectangular shape is more realistic for the tire-pavement contact area. In addition, experimental measurements have shown that the actual loading conditions are non-uniform and depend on the tire construction, tire load, and tire inflation pressure (De Beer 1996). This non-uniform pressure might result due to the stiffening effect of the tire wall. Luo and Prozzi (2005) investigated the effect of the difference between the modeled uniform and the actual distributed pressures on the pavement distress, especially top-down cracking. The authors observed the most significant difference at the pavement surface. Another study by Siddharthan et al. (2002) also reported a significant difference (6 to 30 percent) between the responses computed with uniform and non-uniform contact tire-pavement stress distributions. However, for the case of tensile strain at the bottom of the AC layer, the responses computed with the non-uniform stress distribution are lower. This indicates that the use of uniform load distributions is conservative, at least in the case of the estimation of alligator cracking.

Since it is well documented that the difference in the tire print area configuration is insignificant at greater depths, it was believed that applying a uniform contact pressure over a rectangular tire print area on the pavement surface would be conservative. One advantage of assuming a uniform contact distribution is that the two-solid contact problem was simplified by omitting one of the two solids (i.e., tire) and approximating it by a known stress field. In the field, the actual contact stress between the tire and the pavement is not initially known and depends on the interaction between the tire and the pavement surface. Since pavement responses are of primary interest in this research, the tire was removed, and its interaction was substituted by a known stress field. This allows the local model to be used in different pavement layers, and more realistic time-dependent material properties can be implemented in the analysis.

Contact pressures of the NECEPT truck under different load configurations were calculated from the axle weight and tire print area, as summarized in Table 5. Although different contact pressures may result in different contact areas, for simplicity, averaged dimensions (330 mm by 216 mm) were assumed for all tractor/trailer tires, as shown in Figure 7a. These dimensions correspond to a circular loaded area that has a radius of 150 mm. Uniform contact pressure was then applied on these tire prints.

**Table 5. Summary of contact pressure under different load configurations**

<table>
<tr><th rowspan="2">Axle</th><th rowspan="2" colspan="3">Axle Spacing, m</th><th rowspan="2">Tire</th><th colspan="2">Contact Pressure, kPa</th></tr>
<tr><th>Front Load Configuration</th><th>Back Load Configuration</th></tr>
<tr><td>1</td><td rowspan="2">4.5</td><td></td><td></td><td>single</td><td>454</td><td>441</td></tr>
<tr><td>2</td><td rowspan="2">1.3</td><td></td><td>dual</td><td>580</td><td>384</td></tr>
<tr><td>3</td><td></td><td rowspan="2">5.8</td><td>dual</td><td>550</td><td>408</td></tr>
<tr><td>4</td><td></td><td></td><td>dual</td><td>559</td><td>799</td></tr>
</table>

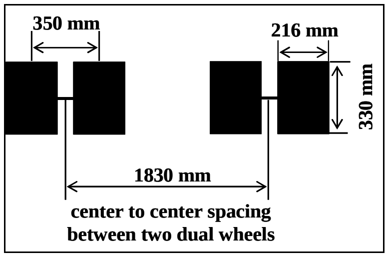


(a) Tire print of the NECEPT truck

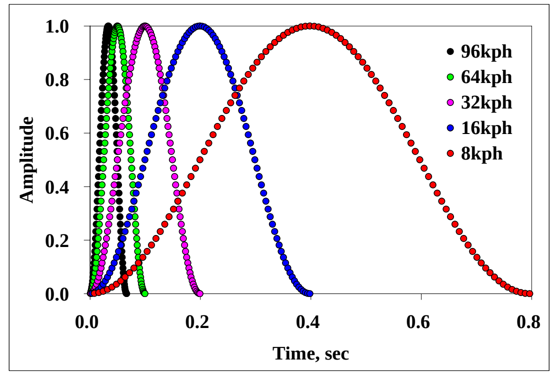


(b) Load amplitude as a function of time

**Figure 7. Simulation of moving load.**

The effect of a moving load on a point in the pavement can be simulated by noting that a time function of the stress can be used to approximate the stress experienced by the point. The relationship between the duration of the moving load and the load amplitude was approximated through a sine function presented by Huang (1993):

$$L(t) = q * \sin^2\left(\frac{\pi}{2} + \frac{\pi}{d}\right) \tag{5}$$

where $t$ is the time of loading, $d$ is the load duration, and $q$ is the load amplitude. When the load is at a considerable distance from a given point, or $t = \pm\, d/2$, the load above the point is zero, or $L(t) = 0$. When the load is directly above the given point, or $t = 0$, the load $L(t) = q$. The duration of the load depends on the vehicle speed $V$ and the tire contact radius $a$. A reasonable assumption is that the load has practically no effect when it is at a distance of $6a$ from the point under consideration. As a result, the load duration $d$ can be computed as $d = (12*a)/V$. For demonstration purposes, load amplitude curves corresponding to target vehicle speeds in the field are shown in Figure 7b. During FE simulations, actual speeds were used. In the FE model, the duration of the load pulse was assumed to not vary through pavement depths. This assumption is not strictly true for pavements in the field. The AASHTO Road Test (1962) showed that the duration of the load pulse increases with increase in the depth at which it is being observed.

Another concern in simulating moving load is the selection of analysis procedure, quasi-static vs. dynamic. A quasi-static loading assumes any dynamic effects of load are reflected in material properties with arbitrary time histories such as relaxation modulus. On the other hand, dynamic analysis accounts for inertial effects in the pavement structure. It was decided to use quasi-static analysis procedures to simulate the field scenario where the moving load approaches and leaves the area of interest; gradual time-steps were employed. A key component of this method is that all calculations are based entirely on known values from the previous time-step. Consequently, relatively small time-steps are required to provide a stable solution. The time-step taken in ABAQUS is fixed instead of automatically computed by the program in order to ensure an accurate solution.

## Element Type

The accuracy of FE solutions depends strongly on the element type used to mesh FE models. In ABAQUS, there are three types of continuum elements available for 3-D FE models: hexahedrons, tetrahedrons, and wedges. There are also linear and quadratic options for each of these basic element shapes. One integration method is “full integration,” which refers to the number of Gauss points required to integrate the polynomial terms in an element’s stiffness matrix exactly when the element has regular shape. The other integration method is called “reduced integration,” which uses one fewer integration point in each direction than the full integration. There is a trade-off between linear and quadratic and also between full integration and reduced integration. In view of the geometric size of the pavement section and preferred accuracy of FE solutions, unbound materials were meshed with 8-node linear brick elements (C3D8R) with reduced integration. This element type has been successfully utilized in FE models for pavement engineering problems (Li and Metcalf 2002, Pirabaroobn et al. 2003). Consequently, these elements act as linear springs to support upper AC layers. Considering the temperature dependency of AC materials, coupled temperature-displacement features that have both displacement and temperature degrees of freedom were also added.

## Optimum Element Size

The FE method is an approximation of the exact solution. Element size needs to be carefully selected since it directly affects the level of accuracy obtained from the FE model. The finest mesh is required near the loads to capture the steep stress and strain gradients. Although the local model could have a very fine mesh, the fineness of element mesh for the global model is also important for cost-effectively obtaining accurate response parameters from local models. The “driven variables” for local models are the solutions from the global model. Computational time and data storage space also need to be considered for the desired level of accuracy. The optimum element size was determined through a mesh refinement analysis that evaluates the virtue of the FE model’s performance in accurately predicting pavement response at multiple depths under a single tire load. It is known that assuming a mesh is convergent just because it has the same element size as a converged mesh in a non-similar model, or at a different location in a similar model, is not valid. Thus, the refinement analysis was performed for Blair and Warren pavement structures separately.

In the FE method, the stresses in an individual element are computed from derivatives of the displacements. The stresses computed from adjacent elements may differ significantly when a coarse element mesh (large element size) is used. The stress differences at the element interfaces (boundaries) decrease as the size of the element is reduced (Bathe 1982). Therefore, a proper FE solution will converge as the number of elements is increased (mesh refinement) to the exact solution. If the stresses are not continuous (large difference) across element boundaries, then the element stresses will not be in equilibrium with externally applied loads. For an ideal continuum pavement system, Bathe’s convergence criteria could be employed at the layer interface such that the optimal computational effort would be achieved through appropriate element sizes.

In the mesh refinement analysis, each pavement layer was first meshed with large elements. This coarse element mesh was then refined by subdividing the previous used element into more elements. With this procedure, the new space of FE interpolation functions contains the previously used space. The element mesh is continuously refined until the vertical stress continuity at layer interfaces is obtained. During this mesh refinement process, linear elastic response of pavement materials was assumed, as listed in Table 6 and 7. Contact pressures of 580 kPa and 790 kPa were uniformly applied over a rectangular tire print area (330 mm by 216 mm) on the pavement surface of Blair and Warren, respectively. These two pressures correspond to the maximum contact pressure values under front and back load configurations (Table 5).

**Table 6. Elastic properties used in mesh refinement analysis for Blair**

| Layer | Thickness, mm | Elastic Modulus, MPa | Poisson's Ratio |
|---|---|---|---|
| Wearing | 54 | 3000 | 0.30 |
| Binder | 47 | 2000 | 0.30 |
| BCBC | 162 | 1000 | 0.30 |
| Subbase | 200 | 500 | 0.35 |
| Subgrade | 2537 | 200 | 0.40 |

**Table 7. Elastic properties used in mesh refinement analysis for Warren**

| Layer | Thickness, mm | Elastic Modulus, MPa | Poisson's Ratio |
|---|---|---|---|
| Wearing | 38 | 3000 | 0.30 |
| Binder | 62 | 2000 | 0.30 |
| BCBC | 138 | 1000 | 0.30 |
| Leveling | 110 | 2000 | 0.30 |
| Fractured PCC | 250 | 500 | 0.35 |
| Subgrade | 2402 | 200 | 0.40 |

Mesh performance was evaluated at points along the vertical axis, which is at the center of the loaded area. Tables 8 to 11 summarize the vertical stress differences for different mesh refinements. A graphic presentation of mesh refinement analyses results is shown in Figure 8. It can be seen that the continuity of vertical stresses at a layer interface is highly affected by the element size of the upper layer. Convergence becomes slower when the element size is smaller than a critical size at refinements 3 (R3) and 4 (R4) for the Blair and Warren models, respectively. This critical element size results in a 5 percent stress difference (29.0 and 39.5 kPa) of applied tire load (580 and 790 kPa). The stress difference is further decreased to 1 percent (5.8 and 7.9 kPa) of applied tire load at refinement 6 (R6) for both models. However, the required computational time and data storage space are extremely high for this level of solution accuracy. Therefore, the cut-boundary displacement method was implemented in the mesh refinement analysis. Continuing with a relatively coarse mesh (global model), much smaller elements were used to mesh a local area (local model), which is directly under the wheel load. Mesh refinement analysis results using the G-L modeling approach are presented in Table 12 and 13. The G-L approach saves a significant amount of the computational time for the current analysis compared with the 3-D FE model without using the cut-boundary displacement method for the same level of accuracy.

Given that an FE model with a 1 percent vertical stress difference at any layer interface would provide an acceptable level of accuracy, optimum element sizes from G-L approach (Table 12 and 13) were applied in all developed models in this study to save in computational time while providing an accurate description of the pavement response.

**Table 8. Mesh refinement analysis results for Blair – I.**

<table>
<tr><th>Mesh Refinement</th><th>Layer</th><th>Element Size, mm</th><th>Number of Elements</th><th>Output File Size, Mbytes</th><th>Computational Time, sec</th><th colspan="4">Vertical Stress Difference at Layer Interface, kPa</th></tr>
<tr><td rowspan="5">R1</td><td>Wearing</td><td>54.0</td><td rowspan="5">9180</td><td rowspan="5">10.5</td><td rowspan="5">49</td><td rowspan="2">73.8</td><td></td><td></td><td></td></tr>
<tr><td>Binder</td><td>47.0</td><td rowspan="2">80.2</td><td></td><td></td></tr>
<tr><td>BCBC</td><td>54.0</td><td></td><td rowspan="2">38.8</td><td></td></tr>
<tr><td>Subbase</td><td>100.0</td><td></td><td></td><td rowspan="2">28.3</td></tr>
<tr><td>Subgrade</td><td>253.0</td><td></td><td></td><td></td></tr>
<tr><td rowspan="5">R2</td><td>Wearing</td><td>27.0</td><td rowspan="5">39400</td><td rowspan="5">72.1</td><td rowspan="5">279</td><td rowspan="2">57.1</td><td></td><td></td><td></td></tr>
<tr><td>Binder</td><td>23.5</td><td rowspan="2">31.4</td><td></td><td></td></tr>
<tr><td>BCBC</td><td>27.0</td><td></td><td rowspan="2">17.9</td><td></td></tr>
<tr><td>Subbase</td><td>40.0</td><td></td><td></td><td rowspan="2">13.0</td></tr>
<tr><td>Subgrade</td><td>126.5</td><td></td><td></td><td></td></tr>
<tr><td rowspan="5">R3</td><td>Wearing</td><td>13.5</td><td rowspan="5">144096</td><td rowspan="5">296.9</td><td rowspan="5">3962</td><td rowspan="2">27.0</td><td></td><td></td><td></td></tr>
<tr><td>Binder</td><td>9.4</td><td rowspan="2">14.0</td><td></td><td></td></tr>
<tr><td>BCBC</td><td>18.0</td><td></td><td rowspan="2">10.1</td><td></td></tr>
<tr><td>Subbase</td><td>20.0</td><td></td><td></td><td rowspan="2">10.6</td></tr>
<tr><td>Subgrade</td><td>126.5</td><td></td><td></td><td></td></tr>
</table>

**Table 9. Mesh refinement analysis results for Blair – II.**

<table>
<tr><th>Mesh Refinement</th><th>Layer</th><th>Element Size, mm</th><th>Number of Elements</th><th>Output File Size, Mbytes</th><th>Computational Time, sec</th><th colspan="4">Vertical Stress Difference at Layer Interface, kPa</th></tr>
<tr><td rowspan="5">R4</td><td>Wearing</td><td>10.8</td><td rowspan="5">249228</td><td rowspan="5">507.5</td><td rowspan="5">12417</td><td rowspan="2">22.6</td><td></td><td></td><td></td></tr>
<tr><td>Binder</td><td>9.4</td><td rowspan="2">14.2</td><td></td><td></td></tr>
<tr><td>BCBC</td><td>18.0</td><td></td><td rowspan="2">10.1</td><td></td></tr>
<tr><td>Subbase</td><td>20.0</td><td></td><td></td><td rowspan="2">6.7</td></tr>
<tr><td>Subgrade</td><td>84.3</td><td></td><td></td><td></td></tr>
<tr><td rowspan="5">R5</td><td>Wearing</td><td>10.8</td><td rowspan="5">353600</td><td rowspan="5">1034.8</td><td rowspan="5">18520</td><td rowspan="2">16.0</td><td></td><td></td><td></td></tr>
<tr><td>Binder</td><td>9.4</td><td rowspan="2">10.9</td><td></td><td></td></tr>
<tr><td>BCBC</td><td>9.0</td><td></td><td rowspan="2">6.8</td><td></td></tr>
<tr><td>Subbase</td><td>20.0</td><td></td><td></td><td rowspan="2">6.2</td></tr>
<tr><td>Subgrade</td><td>84.3</td><td></td><td></td><td></td></tr>
<tr><td rowspan="5">R6</td><td>Wearing</td><td>5.4</td><td rowspan="5">760240</td><td rowspan="5">2156.7</td><td rowspan="5">73143</td><td rowspan="2">4.9</td><td></td><td></td><td></td></tr>
<tr><td>Binder</td><td>4.7</td><td rowspan="2">5.0</td><td></td><td></td></tr>
<tr><td>BCBC</td><td>9.0</td><td></td><td rowspan="2">6.5</td><td></td></tr>
<tr><td>Subbase</td><td>20.0</td><td></td><td></td><td rowspan="2">5.7</td></tr>
<tr><td>Subgrade</td><td>63.3</td><td></td><td></td><td></td></tr>
</table>

**Table 10. Mesh refinement analysis results for Warren – I.**

| Mesh Refinement | Layer | Element Size, mm | Number of Elements | Output File Size, Mbytes | Computational Time, sec | Vertical Stress Different at Layer Interface, kPa | | | | |
|---|---|---|---|---|---|---|---|---|---|---|
| R1 | Wearing | 38.1 | 10530 | 15.5 | 77 | 139.8 | | | | |
| | Binder | 62.2 | | | | | 113.3 | | | |
| | BCBC | 46.1 | | | | | | 42.2 | | |
| | Leveling | 110.5 | | | | | | | 62.1 | |
| | PCC | 125.0 | | | | | | | | 36.7 |
| | Subgrade | 247.0 | | | | | | | | |
| R2 | Wearing | 19.1 | 34000 | 50.8 | 194 | 96.4 | | | | |
| | Binder | 31.1 | | | | | 45.8 | | | |
| | BCBC | 34.6 | | | | | | 26.3 | | |
| | Leveling | 55.2 | | | | | | | 29.5 | |
| | PCC | 62.5 | | | | | | | | 23.9 |
| | Subgrade | 247.0 | | | | | | | | |
| R3 | Wearing | 12.7 | 86690 | 168.4 | 960 | 64.3 | | | | |
| | Binder | 20.7 | | | | | 32.4 | | | |
| | BCBC | 27.7 | | | | | | 22.7 | | |
| | Leveling | 55.2 | | | | | | | 25.4 | |
| | PCC | 50.0 | | | | | | | | 15.4 |
| | Subgrade | 123.5 | | | | | | | | |

**Table 11. Mesh refinement analysis results for Warren – II.**

<table>
<tr><th>Mesh Refinement</th><th>Layer</th><th>Element Size, mm</th><th>Number of Elements</th><th>Output File Size, Mbytes</th><th>Computational Time, sec</th><th colspan="5">Vertical Stress Different at Layer Interface, kPa</th></tr>
<tr><td rowspan="6">R4</td><td>Wearing</td><td>9.5</td><td rowspan="6">185832</td><td rowspan="6">481.7</td><td rowspan="6">5968</td><td rowspan="2">36.4</td><td></td><td></td><td></td><td></td></tr>
<tr><td>Binder</td><td>12.4</td><td rowspan="2">21.1</td><td></td><td></td><td></td></tr>
<tr><td>BCBC</td><td>19.8</td><td></td><td rowspan="2">18.7</td><td></td><td></td></tr>
<tr><td>Leveling</td><td>55.2</td><td></td><td></td><td rowspan="2">17.3</td><td></td></tr>
<tr><td>PCC</td><td>25.0</td><td></td><td></td><td></td><td rowspan="2">9.3</td></tr>
<tr><td>Subgrade</td><td>82.3</td><td></td><td></td><td></td><td></td></tr>
<tr><td rowspan="6">R5</td><td>Wearing</td><td>7.6</td><td rowspan="6">341550</td><td rowspan="6">982.4</td><td rowspan="6">17381</td><td rowspan="2">18.7</td><td></td><td></td><td></td><td></td></tr>
<tr><td>Binder</td><td>10.4</td><td rowspan="2">16.4</td><td></td><td></td><td></td></tr>
<tr><td>BCBC</td><td>14.0</td><td></td><td rowspan="2">8.5</td><td></td><td></td></tr>
<tr><td>Leveling</td><td>36.8</td><td></td><td></td><td rowspan="2">8.4</td><td></td></tr>
<tr><td>PCC</td><td>20.8</td><td></td><td></td><td></td><td rowspan="2">8.7</td></tr>
<tr><td>Subgrade</td><td>82.3</td><td></td><td></td><td></td><td></td></tr>
<tr><td rowspan="6">R6</td><td>Wearing</td><td>3.8</td><td rowspan="6">910396</td><td rowspan="6">3752.4</td><td rowspan="6">118590</td><td rowspan="2">6.2</td><td></td><td></td><td></td><td></td></tr>
<tr><td>Binder</td><td>6.2</td><td rowspan="2">5.5</td><td></td><td></td><td></td></tr>
<tr><td>BCBC</td><td>9.9</td><td></td><td rowspan="2">4.7</td><td></td><td></td></tr>
<tr><td>Leveling</td><td>22.1</td><td></td><td></td><td rowspan="2">5.6</td><td></td></tr>
<tr><td>PCC</td><td>20.8</td><td></td><td></td><td></td><td rowspan="2">8.5</td></tr>
<tr><td>Subgrade</td><td>82.3</td><td></td><td></td><td></td><td></td></tr>
</table>

**Table 12. G-L based mesh refinement analysis results for Blair.**

<table>
<tr><th>Mesh Refinement</th><th>Layer</th><th>Element Size, mm</th><th>Number of Elements</th><th>Output File Size, Mbytes</th><th>Computational Time, sec</th><th colspan="4">Vertical Stress Jump at Layer Interface, kPa</th></tr>
<tr><td rowspan="5">Global (R3)</td><td>Wearing</td><td>13.5</td><td rowspan="5">144096</td><td rowspan="5">296.9</td><td rowspan="5">3962</td><td rowspan="2">27.0</td><td></td><td></td><td></td></tr>
<tr><td>Binder</td><td>9.4</td><td rowspan="2">14.0</td><td></td><td></td></tr>
<tr><td>BCBC</td><td>18.0</td><td></td><td rowspan="2">10.1</td><td></td></tr>
<tr><td>Subbase</td><td>20.0</td><td></td><td></td><td rowspan="2">10.6</td></tr>
<tr><td>Subgrade</td><td>126.5</td><td></td><td></td><td></td></tr>
<tr><td rowspan="5">Local</td><td>Wearing</td><td>5.4</td><td rowspan="5">38880</td><td rowspan="5">82.6</td><td rowspan="5">253</td><td rowspan="2">5.0</td><td></td><td></td><td></td></tr>
<tr><td>Binder</td><td>4.7</td><td rowspan="2">4.8</td><td></td><td></td></tr>
<tr><td>BCBC</td><td>9.0</td><td></td><td rowspan="2">6.2</td><td></td></tr>
<tr><td>Subbase</td><td>10.0</td><td></td><td></td><td rowspan="2">2.5</td></tr>
<tr><td>Subgrade</td><td>20.0</td><td></td><td></td><td></td></tr>
</table>

**Table 13. G-L based mesh refinement analysis results for Warren.**

<table>
<tr><th>Mesh Refinement</th><th>Layer</th><th>Element Size, mm</th><th>Number of Elements</th><th>Output File Size, Mbytes</th><th>Computational Time, sec</th><th colspan="5">Vertical Stress Jump at Layer Interface, kPa</th></tr>
<tr><td rowspan="6">Global (R4)</td><td>Wearing</td><td>9.5</td><td rowspan="6">185832</td><td rowspan="6">481.7</td><td rowspan="6">5968</td><td rowspan="2">36.4</td><td></td><td></td><td></td><td></td></tr>
<tr><td>Binder</td><td>12.4</td><td rowspan="2">21.1</td><td></td><td></td><td></td></tr>
<tr><td>BCBC</td><td>19.8</td><td></td><td rowspan="2">18.7</td><td></td><td></td></tr>
<tr><td>Leveling</td><td>55.2</td><td></td><td></td><td rowspan="2">17.3</td><td></td></tr>
<tr><td>PCC</td><td>25.0</td><td></td><td></td><td></td><td rowspan="2">9.3</td></tr>
<tr><td>Subgrade</td><td>82.3</td><td></td><td></td><td></td><td></td></tr>
<tr><td rowspan="6">Local</td><td>Wearing</td><td>3.8</td><td rowspan="6">37632</td><td rowspan="6">79.9</td><td rowspan="6">210</td><td rowspan="2">6.3</td><td></td><td></td><td></td><td></td></tr>
<tr><td>Binder</td><td>6.2</td><td rowspan="2">5.4</td><td></td><td></td><td></td></tr>
<tr><td>BCBC</td><td>9.9</td><td></td><td rowspan="2">4.9</td><td></td><td></td></tr>
<tr><td>Leveling</td><td>11.0</td><td></td><td></td><td rowspan="2">4.5</td><td></td></tr>
<tr><td>PCC</td><td>12.5</td><td></td><td></td><td></td><td rowspan="2">2.6</td></tr>
<tr><td>Subgrade</td><td>20.0</td><td></td><td></td><td></td><td></td></tr>
</table>

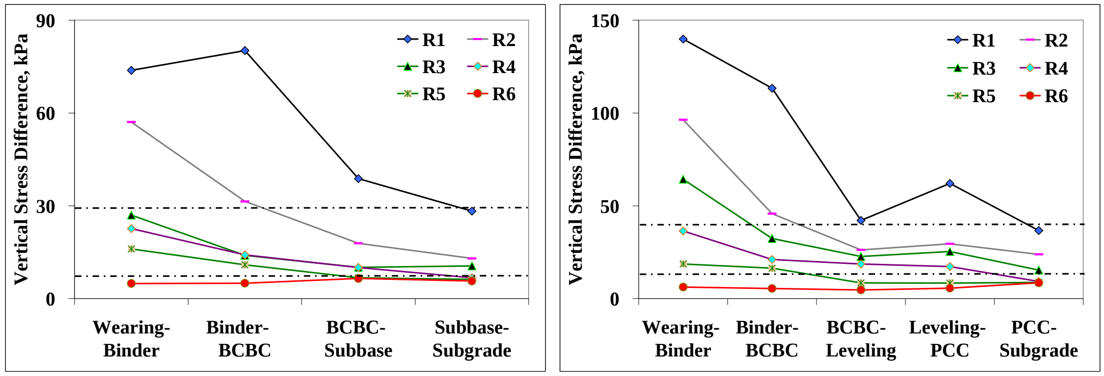


(a) Blair (b) Warren

**Figure 8. Results from mesh refinement analysis**

## Model Dimensions

The determination of the global model's longitudinal dimension is presented in this subsection. The same FE models used in the mesh refinement analyses were employed with a length of 6 m. AC layers were modeled as viscoelastic materials. A lower speed produces a larger duration of loading and subsequently larger dimensions of the stress influence zone. A tire load with 8kph vehicle speed was applied on the pavement surface. This was the lowest target speed in the field. Horizontal strain in longitudinal direction and vertical strains were predicted at various spatial locations. Ideally, the change in these two response parameters with increasing distance from the center of loading area will become negligible for a certain set of plane and vertical dimensions. As an example, predictions of response parameters from the Blair FE model are shown in Figure 9. It is clear from Figure 9a that the FE model provides an acceptable description of longitudinal strain response observed in the field, the compression-tension-compression pattern. Both longitudinal and vertical strain curves follow the same trend that the strain magnitude decreases at deeper locations. This trend was also detected in the field response data. Because the tire load has almost no influence on both strain curves at longitudinal distances more than 2 m from the center of loading area, the longitudinal dimension was set at 4 m for both the Blair and Warren FE global models. All layers were modeled with the same shape to preserve the continuity of nodes at the interface of adjacent layers.

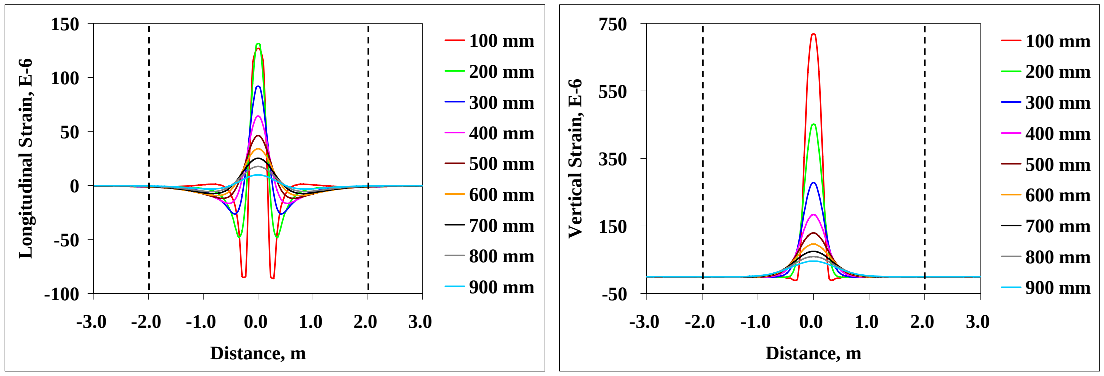


(a) Longitudinal Strain (b) Vertical Strain

**Figure 9. Determination of the longitudinal dimension of the global models**

## Model Validation

Although an effort was made to approach real pavement conditions in the developed FE models based on the available laboratory results and modeling techniques, some approximations were inevitable. Therefore, model validation is an essential step for pavement performance predictions using FE-simulated stress and strain responses. Based on all dynamic measurements collected during the SISSI project, various sets of pavement responses were selected to validate the developed FE models. Selected data sets are shown in Table 14 and Table 15 for Blair and Warren, respectively. These data sets cover various seasons, vehicle speeds, and load configurations. Although strain gauges were also installed at the bottom of the wearing layer at Warren, they stopped responding in 2004. Since other researchers found that the effect of tire wander (between the center of the tire and the instrument) was very significant (Chatti et al. 1996), tire wander was considered in the model validation. An average of two lateral offsets recorded at 7.3 m before and after the centerline of instrumentation was applied in each FE simulation. Both target and actual speeds are reported, but only actual speeds were used to simulate moving loads.

For the SISSI project, all strain gauges were placed in the horizontal plane at the bottom of AC layers. To provide a thorough evaluation of developed FE models, additional response data (i.e., vertical strains) are desirable. A layered elastic analysis (LEA) program, KENLAYER, was used to compute horizontal strains at the bottom of the wearing and leveling layers at Warren and vertical strains in both bound and unbound layers where measured responses are not available. KENLAYER was selected because it is widely accessible and is included with the textbook *Pavement Analysis and Design* (Huang 1993). With time-temperature superposition, for a specific temperature and actual vehicle speed in the field at the time of pavement response measurement, the elastic modulus was obtained from dynamic modulus master curves. These elastic moduli (Tables 16 and 17) were input in KENLAYER. All locations selected for analyses and comparisons are listed in Tables 18 and 19 for Blair and Warren, respectively. Data sources for each response parameter are also reported.

The effectiveness of developed FE models in simulating pavement response is evaluated in terms of the prediction error at peak strains or stresses, *e*:

$$e = \frac{R_{FE} - R_{m(KEN)}}{R_{m(KEN)}} * 100 \tag{6}$$

where $R_{FE}$ is the peak response simulated from FE models, $R_m$ is the peak response measured in the field, and $R_{KEN}$ is the peak response calculated from KENLAYER. A positive value of $e$ indicates an over-prediction from FE simulations, while a negative value of $e$ suggests an under-prediction. Although only prediction errors are reported in this section, a complete summary of measured and FE-simulated pavement responses can be found in Appendix.

**Table 14. Selected response data for Blair.**

| Run # | Season | Date | Time | Target Speed, kph | Actual Speed, kph | Load Configuration | Tire Wander, mm |
|---|---|---|---|---|---|---|---|
| 1 | Spring | 5/4/2004 | 13:36 | 32 | 42 | B | 38 |
| 2 | Summer | 7/20/2004 | 10:32 | 64 | 61 | B | 0 |
| 3 | Summer | 7/20/2004 | 12:25 | 32 | 39 | F | 22 |
| 4 | Fall | 10/21/2004 | 14:35 | 32 | 35 | B | 0 |
| 5 | Fall | 10/21/2004 | 15:06 | 64 | 68 | B | 0 |
| 6 | Spring | 3/7/2005 | 11:22 | 8 | 12 | B | 0 |
| 7 | Spring | 3/7/2005 | 11:33 | 32 | 29 | B | 0 |
| 8 | Spring | 3/7/2005 | 11:58 | 64 | 64 | B | 0 |
| 9 | Spring | 3/7/2005 | 12:57 | 16 | 14 | F | 10 |
| 10 | Spring | 3/7/2005 | 13:30 | 32 | 35 | F | 25 |
| 11 | Spring | 3/7/2005 | 13:42 | 64 | 66 | F | 51 |
| 12 | Summer | 8/23/2005 | 11:32 | 8 | 7 | F | 0 |
| 13 | Summer | 8/23/2005 | 11:49 | 64 | 67 | F | 0 |

**Table 15. Selected response data for Warren.**

| Run # | Season | Date | Time | Target Speed, kph | Actual Speed, kph | Load Configuration | Tire Wander, mm |
|---|---|---|---|---|---|---|---|
| 1 | Summer | 6/27/2003 | 14:00 | 64 | 68 | B | 0 |
| 2 | Summer | 6/27/2003 | 14:21 | 96 | 100 | B | 0 |
| 3 | Summer | 6/27/2003 | 14:29 | 32 | 36 | B | 0 |
| 4 | Summer | 8/24/2004 | 10:33 | 32 | 35 | F | 0 |
| 5 | Summer | 8/24/2004 | 10:57 | 64 | 68 | F | 29 |
| 6 | Summer | 8/24/2004 | 11:10 | 96 | 101 | F | 51 |
| 7 | Summer | 8/24/2004 | 11:56 | 32 | 38 | B | 13 |
| 8 | Summer | 8/24/2004 | 12:12 | 64 | 69 | B | 32 |
| 9 | Summer | 8/24/2004 | 12:30 | 96 | 99 | B | 64 |
| 10 | Fall | 11/5/2004 | 13:06 | 32 | 36 | F | 13 |
| 11 | Fall | 11/5/2004 | 14:12 | 64 | 71 | F | 38 |
| 12 | Fall | 11/5/2004 | 14:31 | 96 | 96 | F | 0 |
| 13 | Fall | 11/5/2004 | 14:54 | 8 | 11 | B | 0 |
| 14 | Fall | 11/5/2004 | 14:56 | 32 | 39 | B | 38 |
| 15 | Fall | 11/5/2004 | 15:06 | 64 | 65 | B | 0 |
| 16 | Fall | 11/5/2004 | 15:16 | 96 | 98 | B | 0 |
| 17 | Spring | 3/17/2005 | 9:52 | 32 | 33 | F | 25 |
| 18 | Spring | 3/17/2005 | 10:05 | 64 | 66 | F | 44 |
| 19 | Spring | 3/17/2005 | 10:32 | 96 | 100 | F | 102 |
| 20 | Spring | 3/17/2005 | 11:05 | 32 | 34 | B | 22 |
| 21 | Spring | 3/17/2005 | 11:10 | 64 | 68 | B | 0 |
| 22 | Spring | 3/17/2005 | 11:29 | 96 | 96 | B | 29 |

**Table 16. Elastic layer moduli for Blair.**

| Run # | Actual Speed, kph | Elastic Layer Moduli | | | | | |
|---|---|---|---|---|---|---|---|
| | | Wearing | | Binder | | BCBC | |
| | | Temp, $^oC$ | \|E*\|, MPa | Temp, $^oC$ | \|E*\|, MPa | Temp, $^oC$ | \|E*\|, MPa |
| 1 | 42 | 31 | 1840 | 28 | 2496 | 18 | 5288 |
| 2 | 61 | 31 | 2106 | 28 | 2844 | 26 | 2688 |
| 3 | 39 | 31 | 1788 | 28 | 2428 | 26 | 2200 |
| 4 | 35 | 13 | 7583 | 13 | 8211 | 12 | 8464 |
| 5 | 68 | 13 | 8717 | 13 | 9438 | 12 | 10136 |
| 6 | 12 | 16 | 4724 | 12 | 6866 | 5 | 10547 |
| 7 | 29 | 16 | 5839 | 12 | 8264 | 5 | 12636 |
| 8 | 64 | 17 | 6697 | 14 | 8878 | 5 | 14652 |
| 9 | 14 | 20 | 3504 | 17 | 4939 | 6 | 10259 |
| 10 | 35 | 21 | 4261 | 18 | 5561 | 6 | 12560 |
| 11 | 66 | 21 | 5057 | 18 | 6527 | 6 | 14142 |
| 12 | 7 | 35 | 613 | 33 | 694 | 29 | 735 |
| 13 | 67 | 37 | 1315 | 33 | 1799 | 29 | 2076 |

**Table 17. Elastic layer moduli for Warren.**

| Run # | Actual Speed, kph | Elastic Layer Moduli | | | | | | | |
|---|---|---|---|---|---|---|---|---|---|
| | | Wearing | | Binder | | BCBC | | Leveling | |
| | | Temp, °C | \|E*\|, MPa | Temp, °C | \|E*\|, MPa | Temp, °C | \|E*\|, MPa | Temp, °C | \|E*\|, MPa |
| 1 | 68 | 39 | 525 | 34 | 2277 | 32 | 2763 | 32 | 2648 |
| 2 | 100 | 41 | 505 | 35 | 2395 | 34 | 2689 | 33 | 2778 |
| 3 | 36 | 41 | 301 | 35 | 1683 | 34 | 1845 | 33 | 1987 |
| 4 | 35 | 31 | 1015 | 24 | 3986 | 22 | 4883 | 22 | 4489 |
| 5 | 68 | 32 | 1228 | 25 | 4466 | 23 | 5469 | 23 | 4993 |
| 6 | 101 | 32 | 1441 | 25 | 4901 | 23 | 5998 | 23 | 5448 |
| 7 | 38 | 38 | 440 | 29 | 2740 | 27 | 3340 | 27 | 3373 |
| 8 | 69 | 38 | 588 | 29 | 3269 | 27 | 3998 | 27 | 3964 |
| 9 | 99 | 40 | 561 | 31 | 3180 | 28 | 4161 | 28 | 3866 |
| 10 | 36 | 11 | 6350 | 9 | 9493 | 8 | 10990 | 8 | 9792 |
| 11 | 71 | 12 | 6950 | 11 | 9438 | 11 | 10590 | 10 | 9737 |
| 12 | 96 | 13 | 7066 | 11 | 9840 | 11 | 11044 | 10 | 10136 |
| 13 | 11 | 12 | 4469 | 12 | 6733 | 10 | 8525 | 9 | 7932 |
| 14 | 39 | 12 | 6086 | 12 | 8342 | 10 | 10375 | 9 | 9549 |
| 15 | 65 | 12 | 6848 | 12 | 9046 | 10 | 11161 | 9 | 10239 |
| 16 | 98 | 12 | 7428 | 12 | 9563 | 10 | 11730 | 9 | 10741 |
| 17 | 33 | 7 | 8243 | 3 | 11694 | 2 | 13430 | 1 | 12503 |
| 18 | 66 | 7 | 9256 | 3 | 12478 | 2 | 14250 | 1 | 13245 |
| 19 | 100 | 10 | 8511 | 5 | 12177 | 4 | 14212 | 3 | 12960 |
| 20 | 34 | 11 | 6222 | 8 | 9674 | 7 | 11524 | 5 | 10848 |
| 21 | 68 | 11 | 7253 | 8 | 10591 | 7 | 12527 | 5 | 11725 |
| 22 | 96 | 14 | 6403 | 9 | 10720 | 7 | 9680 | 6 | 11847 |

**Table 18. Summary of analysis locations for Blair.**

| Analysis Location | Depth, mm | Response Parameter | | |
|---|---|---|---|---|
| | | Horizontal Strain | Vertical Stress | Vertical Strain |
| Bottom of Wearing | 54 | Measured | - | KENLAYER |
| Bottom of Binder | 101 | Measured | - | KENLAYER |
| Bottom of BCBC | 263 | Measured | - | KENLAYER |
| Top of Subbase | 263 | - | Measured | KENLAYER |
| Top of Subgrade | 463 | - | Measured | KENLAYER |

**Table 19. Summary of analysis locations for Warren.**

| Analysis Location | Depth, mm | Response Parameter | |
|---|---|---|---|
| | | Horizontal Strain | Vertical Strain |
| Bottom of Wearing | 38 | KENLAYER | KENLAYER |
| Bottom of Binder | 100 | Measured | KENLAYER |
| Bottom of BCBC | 239 | Measured | KENLAYER |
| Bottom of Leveling | 349 | KENLAYER | KENLAYER |
| Top of Fractured PCC | 349 | KENLAYER | KENLAYER |
| Top of Subgrade | 599 | KENLAYER | KENLAYER |

## Comparison of FEA and Measured Responses

### Blair FE Model

Based on the function and location of instrumented dynamic sensors, prediction errors are tabulated in Tables 20 and 21 for strains in the AC layers and stresses in the unbound layers, respectively. In general, the Blair FE model seems to under-predict pavement responses in AC materials. The main conclusions of strain predictions can be made as follows:

- FE model is capable of simulating pavement responses under different load configurations.
- FE model results in a slightly larger prediction error at the bottom of the wearing layer. This is possibly due the simplification of contact pressure distribution at the pavement surface.
- FE model predicts smaller strains (a larger prediction error) during warm seasons. Since AC materials are modeled in viscoelastic mode, experiment tests

other than the complex modulus test, such as the creep-recovery test, are needed to capture the viscoplastic behavior of AC such that the accuracy of strain predictions at high temperatures can be improved.
- One interesting observation in Table 20 is that strain responses under axle 3 are much smaller than field-measured values, particularly at higher speeds, i.e., 64 kph. This phenomenon is shown in Figure 10a. Iif the next pass of the tire load comes before the complete relaxation of strains has taken place, the unrecovered inelastic (residual) strains may cause permanent deformation. From the dimensions of the NECEPT truck (Table 5), the axle spacing between axle 2 (second axle of the tractor) and 3 (first axle of the trailer) is much shorter than the other two axle spacings. At 64 kph, a travel time of 0.073 sec may not be enough for the pavement to rebound before the arrival of the third pass of the tire load.

On the other hand, the Blair FE model always over-predicts response in granular materials. The main conclusions of stress predictions can be made as follows:

- No obvious dependency of prediction error on load configuration, axle, and vehicle speed has been observed.
- The prediction error decreases as deeper points in the pavement are considered.
- Prediction errors are quite large in the summer. This is probably due to the low subbase modulus backcalculated from FWD data (Table 3). Further improvements on the accuracy of stress response prediction require soil characterization tests, such as the resilient modulus test.

For all the selected response data sets, the FE model accuracy is acceptable, with an overall error of -11.2 percent in predicting longitudinal strains and 14.3 percent in predicting vertical stresses. Hence, the assessment is that the Blair FE model provides a satisfactory prediction of pavement response to vehicular loading.

## Warren FE Model

Because no pressure cells were installed at Warren, only strain prediction errors are summarized in Table 22. Similarly to the Blair FE model, the Warren FE model seems to under-predict pavement responses in AC materials. However, an overall prediction error of -7.8 percent suggests a better agreement between measured and predicted longitudinal strains. Several conclusions of strain predictions can be made as follows:

- Load configuration (front vs. back) has no impact on strain predictions.
- The trend that the prediction error is smaller at a deeper location is not clear.
- The inability to simulate strain responses at high temperature is apparent due to the viscoelastic mode included in the FE model.
- Potential permanent deformations occur between the second and third passes of tire load, as shown in Figure 10b. At the highest vehicle speed (96kph), the

time gap between the middle two axles of the tractor trailer is only 0.049sec.

**Table 20. Summary of strain prediction errors (%) of Blair FE model.**

| Analysis Conditions | | Prediction Error, % |
|---|---|---|
| Overall | | -11.2 |
| Load Configuration | Front | -11.1 |
| | Back | -11.3 |
| Analysis Location | Bottom of Wearing | -13.1 |
| | Bottom of Binder | -10.5 |
| | Bottom of BCBC | -10.0 |
| Season | Spring | -9.5 |
| | Summer | -14.3 |
| | Fall | -9.9 |
| Axle | 1 | -10.5 |
| | 2 | -10.5 |
| | 3 | -13.7 |
| | 4 | -10.4 |
| Vehicle Speed, kph | 8 | -10.6 |
| | 16 | -10.9 |
| | 32 | -11.2 |
| | 64 | -12.3 |

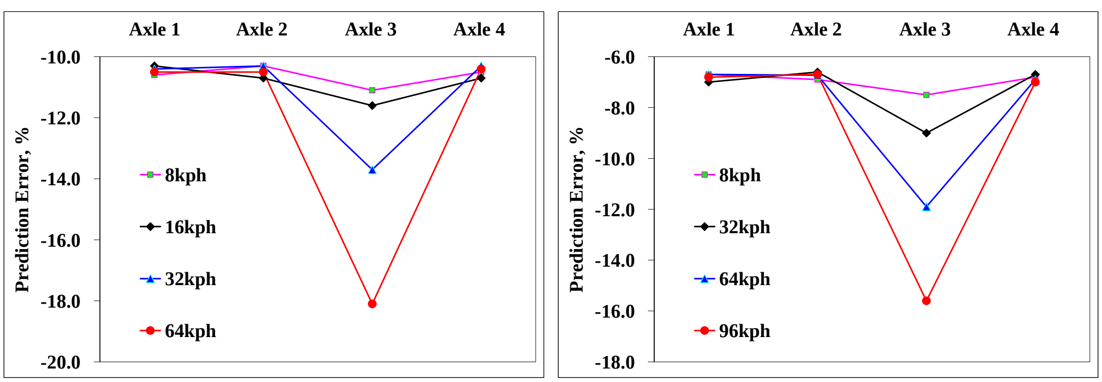


(a) Blair (b) Warren

**Figure 10. Prediction errors for different axles and target speeds**

**Table 21. Summary of stress prediction errors (%) of Blair FE model.**

| Analysis Conditions | | Prediction Error, % |
|---|---|---|
| Overall | | 14.3 |
| Load Configuration | Front | 14.3 |
| | Back | 14.3 |
| Analysis Location | Top of Subbase | 15.1 |
| | Top of Subgrade | 13.5 |
| Season | Spring | 13.0 |
| | Summer | 16.4 |
| | Fall | 13.5 |
| Axle | 1 | 14.3 |
| | 2 | 14.2 |
| | 3 | 14.3 |
| | 4 | 14.4 |
| Vehicle Speed, kph | 8 | 14.1 |
| | 16 | 14.5 |
| | 32 | 14.0 |
| | 64 | 14.4 |

**Table 22. Summary of strain prediction errors (%) of Warren FE model.**

| Analysis Conditions | | Prediction Error, % |
|---|---|---|
| Overall | | -7.8 |
| Load Configuration | Front | -7.8 |
| | Back | -7.8 |
| Analysis Location | Bottom of Binder | -7.9 |
| | Bottom of BCBC | -7.7 |
| Season | Spring | -6.6 |
| | Summer | -10.5 |
| | Fall | -6.3 |
| Axle | 1 | -6.8 |
| | 2 | -6.7 |
| | 3 | -11.0 |
| | 4 | -6.9 |
| Vehicle Speed, kph | 16 | -7.0 |
| | 32 | -7.3 |
| | 64 | -8.1 |
| | 96 | -9.0 |

**Comparison of FEA and KENLAYER**

Horizontal strains at deeper locations of bound layers and vertical strains in unbound layers were not captured by field instrumentation at the SISSI sites. To further verify the developed FE models, the responses at these locations from FE solutions were compared with LEA solutions. Comparisons were only made with strain responses under the fourth axle of the NECEPT truck. A radius of 150mm was chosen for the circular contact area in KENLAYER. This radius corresponds to an equivalent contact area as measured for the NECEPT truck.

Tables 23 to 25 summarize the prediction errors of FE models as compared to LEA solutions from KENLAYER. As shown in these tables, FE models have poor agreement with KENLAYER. In general, FE models seem to underpredict both vertical strains and horizontal strains regardless of load configurations. An overall prediction error is about 22 percent for vertical strains and 35 percent for horizontal strains.
Several conclusions on vertical strain predictions can be made as follows:

- No obvious dependency of prediction error on vehicle speed has been observed.
- Prediction errors are relatively larger in summer than in spring and fall.

Several conclusions on horizontal strain predictions can be made as follows:

- Prediction error is highly dependent upon the analysis location, vehicle speed, and pavement temperature.
- The prediction error of horizontal strains decreases as deeper points in the pavement are considered. This is probably due to the viscoelastic nature of AC materials, whereas the elastic mode is incorporated into KENLAYER.

**Table 23. Summary of vertical strain prediction errors (%) from Blair FE model.**

| Analysis Conditions | | Prediction Error, % |
|---|---|---|
| Overall | | -22.4 |
| Load Configuration | Front | -23.8 |
| | Back | -21.0 |
| Analysis Location | Top of Binder | -26.0 |
| | Top of BCBC | -22.0 |
| | Top of Subbase | -21.2 |
| | Top of Subgrade | -20.6 |
| Season | Spring | -20.1 |
| | Summer | -26.4 |
| | Fall | -20.6 |
| Vehicle Speed, kph | 8 | -22.4 |
| | 16 | -22.5 |
| | 32 | -22.5 |
| | 64 | -22.3 |

**Table 24. Summary of horizontal strain prediction errors (%) from Warren FE model.**

| Analysis Conditions | | Prediction Error, % |
|---|---|---|
| Overall | | -35.6 |
| Load Configuration | Front | -35.2 |
| | Back | -36.3 |
| Analysis Location | Bottom of Wearing | -37.4 |
| | Bottom of Leveling | -33.8 |
| Season | Spring | -34.8 |
| | Summer | -39.4 |
| | Fall | -32.8 |
| Vehicle Speed, kph | 8 | -37.9 |
| | 16 | -37.1 |
| | 32 | -34.0 |
| | 64 | -32.8 |

**Table 25. Summary of vertical strain prediction errors (%) from Warren FE model.**

| Analysis Conditions | | Prediction Error, % |
|---|---|---|
| Overall | | -22.3 |
| Load Configuration | Front | -22.0 |
| | Back | -22.5 |
| Analysis Location | Top of Binder | -26.7 |
| | Top of BCBC | -23.5 |
| | Top of Leveling | -20.8 |
| | Top of Fracture PCC | -20.3 |
| | Top of Subgrade | -20.1 |
| Season | Spring | -20.0 |
| | Summer | -24.1 |
| | Fall | -22.4 |
| Vehicle Speed, kph | 8 | -21.2 |
| | 16 | -22.9 |
| | 32 | -22.9 |
| | 64 | -22.5 |

## Linearity of Pavement Response

As discussed in previous sections, linear viscoelastic and elastic behaviors were assumed for bound and unbound materials. These assumptions imply that the response (stress or strain) is linearly proportional to the applied load. That is, as the load increases or decreases on the pavement surface, the response at a given point will increase or decrease linearly. In order to verify the above assumption of linearity, two sets of analysis were conducted using the developed Blair and Warren FE models separately. To exclude the tire wander effect, three runs were first selected from Tables 14 (runs # 4, 8, and 12) and 15 (runs # 3, 13, and 21). These runs cover all three seasons in which dynamic data were collected in the field. Then, for each run, the contact pressure was increased at a 100-kPa interval while vehicle speed and pavement temperature were kept constant. FE-simulated strain responses at various load levels are shown in Figure 11 and Figure 12. Figure 11 shows the tensile strains at the bottom of the BCBC layer, whereas Figure 12 shows the compressive strains at the top of the subgrade as a function of load level. Responses at these two locations are critical for the determination of distresses, such as fatigue cracking and permanent deformation in the respective layers. The linear relationship between the contact pressure and the response clearly validates the assumption of linearity. For both Blair and Warren FE models, as the load increases, the response also increases proportionally. As expected, this trend is pronounced at higher temperatures, which results in lower stiffness of AC materials.

In the case of computing pavement responses under real traffic conditions, the linear relationship between load and response can be used to reduce the computational cost. For example, if the axle load of passing vehicles is known, then the responses for the entire load spectrum can be obtained by load proportionality. More details on such applications are covered in the next chapter.

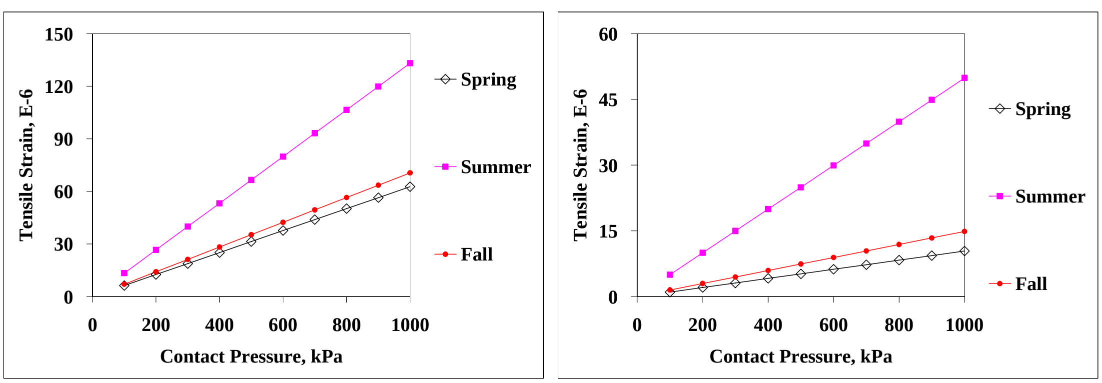


(a) Blair, BCBC (b) Warren, Leveling

**Figure 11. Tensile strains at the bottom of the last AC layer**

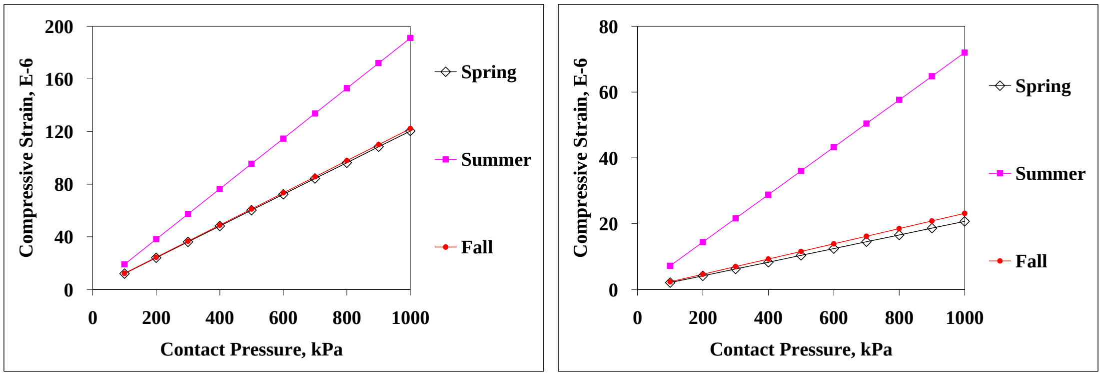


(a) Blair (b) Warren

**Figure 12. Compressive strains at the top of subgrade**

## Summary

This report presents an application of 3-D FE models of two AC pavement structures to simulate pavement responses to multiple axle loads with different load configurations, vehicle speeds, and seasons. Key FE modeling parameters such as model dimensions, material properties, load and boundary conditions, element type, and mesh refinement are covered in detail. Each of these factors affects the overall FEA efficiency. In the FE model, bound materials were modeled in a viscoelastic mode, and unbound materials were modeled in an elastic mode. With appropriate element type and mesh density, developed FE models provide acceptable predictions of pavement response as compared to field-measured values and LEA solutions. The adopted Global-Local (G-L) FE modeling strategy has been shown to be effective in reducing computational cost and obtaining accurate predictions.

## References

ABAQUS/Standard User’s Manual (2002) Finite Element Computer Program. Hibbitt, Karlsson and Sorenson, Inc., Pawtucket, RI, USA, Version 6.3.

Ahmed, Z., Marukic, I., Zaghloul, S., and Vitillo, N. (2005) “Validation of Enhanced Integrated Climatic Model Predictions Using New Jersey Seasonal Monitoring Data.” Paper presented at 84th Annual Meeting, Transportation Research Board, Washington D.C.

Bathe, K. J. (1982) Finite Element Procedures in Engineering Analysis, Prentice-Hall, NJ.

Birgisson, B., Ovik, J., and Newcomb, D. (2000) “Analytical Predictions of Seasonal Variations in Flexible Pavements at the Mn/Road Site.” *Transportation Research Record No. 1730*, National Research Council, Washington, D.C.

Chatti, K., Kim, H.B., Yun, K.K., Mahoney, J.P. and Monismith, C.L. (1996) “Field Investigation into Effects of Vehicle Speed and Tire Pressure on Asphalt Concrete Pavement Strains.” *Transportation Research Record No. 1539*, Transportation Research Board, Washington, D.C.

Chen, D.H., Zaman, M., Laguros, J., and Soltani, A. (1995) “Assessment of Computer Programs for Analysis of Flexible Pavement Structures.” *Transportation Research Record 1539*, Transportation Research Board, Washington, DC.

Cho, Y.H., McCullough, B.F., and Weissmann, J. (1996) “Considerations on Finite-Element Method Application in Pavement Structural Analysis.” *Transportation Research Record 1539*, Transportation Research Board, Washington, DC.

De Beer, M. (1996) Measurement of Tyre/Pavement Interface Stresses under Moving Wheel Loads. *Int. J. of Vehicle Design. Vol. 3.*

De Jong, D.L., Peatz, M.G.F., and Korswagen, A.R. (1973) *Computer Program Bisar Layered System Under Normal and Tangential Loads*. Konin Klijke Shell-Laboratorium, Amsterdam, Netherlands.

ERES Consultants Division. (2004) *Guide for Mechanistic-Empirical Design of New and Rehabilitated Pavement Structures*. Final Report NCHRP 1-37A, Champaign, IL.

Heydinger, A.G. (2003) *Monitoring Seasonal Instrumentation and Modeling Climatic Effects on Pavements at the Ohio/SHRP Test Road*. Final Report, Report No FHWA/OH-2003/018, Department of Civil Engineering, The University of Toledo, Toledo, OH.

Hjelmsted, K.D., Kim, J., and Zuo, Q. (1997) “Finite Element Procedures for Three Dimensional Pavement Analysis.” *Aircraft/Pavement Technology: In the Midst of Chang, Proceedings*, ASCE Airfield Pavement Conference, Seattle, WA.

Huang, Y. (1993) Pavement Analysis and Design. Prentice Hall, NJ.

Kuo, M. C., Hall, K. T., and Darter, M. (1995) “Three-dimensional Finite Element Model for Analysis of Concrete Pavement Support.” *Transportation Research Record No. 1505*, Transportation Research Board, Washington, D.C.

Li, Y. and Metcalf, J.B. (2002) “Crack Initiation Model from Asphalt Slab Tests.” *Journal of Materials in Civil Engineering*, ASCE.

Larson, G. and Dempsey, B. J. (1997) *Enhanced Integrated Climatic Model, Version 2.0*. Final Report, Contract DTFA MN/DOT 72114, Department of Civil Engineering, University of Illinois at Urbana-Champaign, Urbana, IL.

Liang, Robert Y., Rabab’ah, S., Al-Akhras, K. (2006) “Validation of Enhanced Integrated Climatic Model Prediction Over Different Drainable Base Materials.”

presented at 85th Annual Meeting, Transportation Research Board, Washington D.C.

Luo, R. and Prozzi, J. (2005) *Evaluation of the Joint Effect of Wheel Load and Tire Pressure on Pavement Performance*. Center for Transportation Research, University of Texas at Austin, TX.

Lukanen, Erland O., Stubstad, R., Briggs, R. (2000) *Temperature Predictions and Adjustment Factors for Asphalt Pavements*. Report FHWA-RD-98-085, Federal Highway Administration, McLean, VA.

Lytton, R.L., Pufahl, D.E., Michalak, C. H., Liang, H. S., and Dempsey, B. J. (1990) *An Integrated Model of the Climatic Effects on Pavement*. Texas Transportation Institute, Texas A&M University, Report No FHWA-RD-90-033, 1990, Federal Highway Administration, McLean, VA.

Marshall, C., Meier, R., and Weilch M. (2001) "Seasonal Temperature Effects on Flexible Pavements in Tennessee." *Transportation Research Record No. 1764*, Transportation Research Board, Washington, D.C.

Pirabaroobn, S., Zaman, M., and Tarefder, R.A. (2003) "Evaluation of Rutting Potential in Asphalt Mixes Using Finite Element Modeling." 2003 Annual Conference of the Transportation Association of Canada, St. John's, Newfoundland and Labrador, USA.

Schapery, R. and Park, S. (1999) "Methods of Interconversion Between Linear Viscoelastic Material Functions. Part II – An Approximate Analytical Method." *International Journal of Solids and Structures, Vol. 36*.

Shoukry, S. (1998a) "3D Finite Element Modeling for Pavement Analysis and Design." *Proceedings, First National Symposium on 3D Finite Element Modeling for Pavement Analysis and Design*, Charleston, WV.

Siddharthan, Raj V., Krishnamenon, N., El-Mously, M., and Sebaaly, Peter E. (2002) "Investigation of Tire Contact Stress Distributions on Pavement Response." *J. Transp. Engrg., Vol. 128, Issue 2.*

The AASHTO Road Test (1962) *Report 6 – Special Studies*, HRB Spec. Report 61F.

Uddin, W. (1998) "Application of 3D Finite Element Dynamic Analysis for Pavement Evaluation." *Proceedings, First National Symposium on 3D Finite Element Modeling for Pavement Analysis and Design*, Charleston, WV.

White, T. (1998) "Application of Finite Element Analysis to Pavement Problems." *Proceedings, First National Symposium on 3D Finite Element Modeling for Pavement Analysis and Design*, Charleston, WV.

Zaghloul, S. M., and White, T. D. (1993) "Use of a Three-dimensional, Dynamic Finite Element Program for Analysis of Flexible Pavement." *Transportation Research Record No. 1388*, Transportation Research Board, Washington, D.C.

Zaghloul, S., Gucunski, N., Jackson, H., and Hadidi, R. (2006) *Material Characterization and Seasonal Variation in Material Properties*. Final Report, Report No FHWA NJ-2005-024, Center for Advanced Infrastructure and Transportation, Dept. of Civil & Environmental Engineering, Rutgers, the State University, Piscataway, NJ.

## Appendix: Validation Results of FE Models

**Table 1. Summary of measured and FE simulated horizontal strains for Blair.**

| Run# | Load Configuration | Location | Season | Axle | Actual Speed, kph | Data Source | Strain, E-6 |
|---|---|---|---|---|---|---|---|
| 1 | B | Wearing | Spring | 1 | 42 | Measured | 32.6 |
| 1 | B | Wearing | Spring | 1 | 42 | Predicted | 29.0 |
| 1 | B | Wearing | Spring | 2 | 42 | Measured | 13.9 |
| 1 | B | Wearing | Spring | 2 | 42 | Predicted | 12.4 |
| 1 | B | Wearing | Spring | 3 | 42 | Measured | 14.9 |
| 1 | B | Wearing | Spring | 3 | 42 | Predicted | 13.2 |
| 1 | B | Wearing | Spring | 4 | 42 | Measured | 56.8 |
| 1 | B | Wearing | Spring | 4 | 42 | Predicted | 50.5 |
| 1 | B | Binder | Spring | 1 | 42 | Measured | 22.1 |
| 1 | B | Binder | Spring | 1 | 42 | Predicted | 19.8 |
| 1 | B | Binder | Spring | 2 | 42 | Measured | 16.2 |
| 1 | B | Binder | Spring | 2 | 42 | Predicted | 14.5 |
| 1 | B | Binder | Spring | 3 | 42 | Measured | 15.3 |
| 1 | B | Binder | Spring | 3 | 42 | Predicted | 13.6 |
| 1 | B | Binder | Spring | 4 | 42 | Measured | 41.1 |
| 1 | B | Binder | Spring | 4 | 42 | Predicted | 36.8 |
| 1 | B | BCBC | Spring | 2 | 42 | Measured | 15.8 |
| 1 | B | BCBC | Spring | 2 | 42 | Predicted | 14.1 |
| 1 | B | BCBC | Spring | 3 | 42 | Measured | 17.6 |
| 1 | B | BCBC | Spring | 3 | 42 | Predicted | 15.6 |
| 1 | B | BCBC | Spring | 4 | 42 | Measured | 22.7 |
| 1 | B | BCBC | Spring | 4 | 42 | Predicted | 20.3 |
| 2 | B | Wearing | Summer | 1 | 61 | Measured | 22.8 |
| 2 | B | Wearing | Summer | 1 | 61 | Predicted | 20.0 |
| 2 | B | Wearing | Summer | 2 | 61 | Measured | 10.7 |
| 2 | B | Wearing | Summer | 2 | 61 | Predicted | 9.4 |

| | | | | | | | |
|---|---|---|---|---|---|---|---|
| 2 | B | Wearing | Summer | 3 | 61 | Measured | 8.5 |
| 2 | B | Wearing | Summer | 3 | 61 | Predicted | 7.4 |
| 2 | B | Wearing | Summer | 4 | 61 | Measured | 39.5 |
| 2 | B | Wearing | Summer | 4 | 61 | Predicted | 34.7 |
| 2 | B | Binder | Summer | 1 | 61 | Measured | 12.7 |
| 2 | B | Binder | Summer | 1 | 61 | Predicted | 11.2 |
| 2 | B | Binder | Summer | 2 | 61 | Measured | 6.3 |
| 2 | B | Binder | Summer | 2 | 61 | Predicted | 5.6 |
| 2 | B | Binder | Summer | 3 | 61 | Measured | 5.3 |
| 2 | B | Binder | Summer | 3 | 61 | Predicted | 4.6 |
| 2 | B | Binder | Summer | 4 | 61 | Measured | 21.8 |
| 2 | B | Binder | Summer | 4 | 61 | Predicted | 19.2 |
| 2 | B | BCBC | Summer | 1 | 61 | Measured | 13.3 |
| 2 | B | BCBC | Summer | 1 | 61 | Predicted | 11.8 |
| 2 | B | BCBC | Summer | 2 | 61 | Measured | 9.0 |
| 2 | B | BCBC | Summer | 2 | 61 | Predicted | 8.0 |
| 2 | B | BCBC | Summer | 3 | 61 | Measured | 9.3 |
| 2 | B | BCBC | Summer | 3 | 61 | Predicted | 8.1 |
| 2 | B | BCBC | Summer | 4 | 61 | Measured | 11.1 |
| 2 | B | BCBC | Summer | 4 | 61 | Predicted | 9.8 |
| 3 | F | Wearing | Summer | 1 | 39 | Measured | 56.4 |
| 3 | F | Wearing | Summer | 1 | 39 | Predicted | 49.6 |
| 3 | F | Wearing | Summer | 2 | 39 | Measured | 38.6 |
| 3 | F | Wearing | Summer | 2 | 39 | Predicted | 33.9 |
| 3 | F | Wearing | Summer | 3 | 39 | Measured | 40.3 |
| 3 | F | Wearing | Summer | 3 | 39 | Predicted | 35.2 |
| 3 | F | Wearing | Summer | 4 | 39 | Measured | 50.3 |
| 3 | F | Wearing | Summer | 4 | 39 | Predicted | 44.2 |
| 3 | F | Binder | Summer | 1 | 39 | Measured | 24.2 |
| 3 | F | Binder | Summer | 1 | 39 | Predicted | 21.4 |
| 3 | F | Binder | Summer | 2 | 39 | Measured | 29.4 |

| | | | | | | | |
|---|---|---|---|---|---|---|---|
| 3 | F | Binder | Summer | 2 | 39 | Predicted | 26.0 |
| 3 | F | Binder | Summer | 3 | 39 | Measured | 26.1 |
| 3 | F | Binder | Summer | 3 | 39 | Predicted | 22.9 |
| 3 | F | Binder | Summer | 4 | 39 | Measured | 31.8 |
| 3 | F | Binder | Summer | 4 | 39 | Predicted | 28.1 |
| 3 | F | BCBC | Summer | 1 | 39 | Measured | 24.3 |
| 3 | F | BCBC | Summer | 1 | 39 | Predicted | 21.5 |
| 3 | F | BCBC | Summer | 2 | 39 | Measured | 14.3 |
| 3 | F | BCBC | Summer | 2 | 39 | Predicted | 12.6 |
| 3 | F | BCBC | Summer | 3 | 39 | Measured | 17.9 |
| 3 | F | BCBC | Summer | 3 | 39 | Predicted | 15.7 |
| 3 | F | BCBC | Summer | 4 | 39 | Measured | 23.3 |
| 3 | F | BCBC | Summer | 4 | 39 | Predicted | 20.6 |
| 4 | B | Wearing | Fall | 1 | 35 | Measured | 18.4 |
| 4 | B | Wearing | Fall | 1 | 35 | Predicted | 16.3 |
| 4 | B | Wearing | Fall | 2 | 35 | Measured | 8.1 |
| 4 | B | Wearing | Fall | 2 | 35 | Predicted | 7.2 |
| 4 | B | Wearing | Fall | 3 | 35 | Measured | 9.3 |
| 4 | B | Wearing | Fall | 3 | 35 | Predicted | 8.2 |
| 4 | B | Wearing | Fall | 4 | 35 | Measured | 31.2 |
| 4 | B | Wearing | Fall | 4 | 35 | Predicted | 27.7 |
| 4 | B | Binder | Fall | 1 | 35 | Measured | 6.9 |
| 4 | B | Binder | Fall | 1 | 35 | Predicted | 6.2 |
| 4 | B | Binder | Fall | 2 | 35 | Measured | 4.9 |
| 4 | B | Binder | Fall | 2 | 35 | Predicted | 4.4 |
| 4 | B | Binder | Fall | 3 | 35 | Measured | 5.3 |
| 4 | B | Binder | Fall | 3 | 35 | Predicted | 4.7 |
| 4 | B | Binder | Fall | 4 | 35 | Measured | 10.2 |
| 4 | B | Binder | Fall | 4 | 35 | Predicted | 9.1 |
| 4 | B | BCBC | Fall | 1 | 35 | Measured | 4.8 |
| 4 | B | BCBC | Fall | 1 | 35 | Predicted | 4.3 |

| | | | | | | | |
|---|---|---|---|---|---|---|---|
| 4 | B | BCBC | Fall | 2 | 35 | Measured | 2.3 |
| 4 | B | BCBC | Fall | 2 | 35 | Predicted | 2.1 |
| 4 | B | BCBC | Fall | 3 | 35 | Measured | 2.3 |
| 4 | B | BCBC | Fall | 3 | 35 | Predicted | 2.0 |
| 4 | B | BCBC | Fall | 4 | 35 | Measured | 8.2 |
| 4 | B | BCBC | Fall | 4 | 35 | Predicted | 7.3 |
| 5 | B | Wearing | Fall | 1 | 68 | Measured | 8.9 |
| 5 | B | Wearing | Fall | 1 | 68 | Predicted | 7.9 |
| 5 | B | Wearing | Fall | 2 | 68 | Measured | 4.5 |
| 5 | B | Wearing | Fall | 2 | 68 | Predicted | 4.0 |
| 5 | B | Wearing | Fall | 3 | 68 | Measured | 3.0 |
| 5 | B | Wearing | Fall | 3 | 68 | Predicted | 2.6 |
| 5 | B | Wearing | Fall | 4 | 68 | Measured | 16.7 |
| 5 | B | Wearing | Fall | 4 | 68 | Predicted | 14.8 |
| 5 | B | Binder | Fall | 1 | 68 | Measured | 2.8 |
| 5 | B | Binder | Fall | 1 | 68 | Predicted | 2.5 |
| 5 | B | Binder | Fall | 2 | 68 | Measured | 1.9 |
| 5 | B | Binder | Fall | 2 | 68 | Predicted | 1.7 |
| 5 | B | Binder | Fall | 3 | 68 | Measured | 1.7 |
| 5 | B | Binder | Fall | 3 | 68 | Predicted | 1.5 |
| 5 | B | Binder | Fall | 4 | 68 | Measured | 5.1 |
| 5 | B | Binder | Fall | 4 | 68 | Predicted | 4.5 |
| 5 | B | BCBC | Fall | 1 | 68 | Measured | 3.3 |
| 5 | B | BCBC | Fall | 1 | 68 | Predicted | 2.9 |
| 5 | B | BCBC | Fall | 2 | 68 | Measured | 2.2 |
| 5 | B | BCBC | Fall | 2 | 68 | Predicted | 2.0 |
| 5 | B | BCBC | Fall | 3 | 68 | Measured | 0.5 |
| 5 | B | BCBC | Fall | 3 | 68 | Predicted | 0.4 |
| 5 | B | BCBC | Fall | 4 | 68 | Measured | 5.5 |
| 5 | B | BCBC | Fall | 4 | 68 | Predicted | 4.9 |
| 6 | B | Wearing | Spring | 1 | 12 | Measured | 26.3 |

| | | | | | | | |
|---|---|---|---|---|---|---|---|
| 6 | B | Wearing | Spring | 1 | 12 | Predicted | 23.4 |
| 6 | B | Wearing | Spring | 2 | 12 | Measured | 12.2 |
| 6 | B | Wearing | Spring | 2 | 12 | Predicted | 10.9 |
| 6 | B | Wearing | Spring | 3 | 12 | Measured | 13.5 |
| 6 | B | Wearing | Spring | 3 | 12 | Predicted | 11.9 |
| 6 | B | Wearing | Spring | 4 | 12 | Measured | 40.9 |
| 6 | B | Wearing | Spring | 4 | 12 | Predicted | 36.4 |
| 6 | B | Binder | Spring | 1 | 12 | Measured | 14.4 |
| 6 | B | Binder | Spring | 1 | 12 | Predicted | 12.9 |
| 6 | B | Binder | Spring | 2 | 12 | Measured | 8.0 |
| 6 | B | Binder | Spring | 2 | 12 | Predicted | 7.2 |
| 6 | B | Binder | Spring | 3 | 12 | Measured | 6.5 |
| 6 | B | Binder | Spring | 3 | 12 | Predicted | 5.8 |
| 6 | B | Binder | Spring | 4 | 12 | Measured | 19.7 |
| 6 | B | Binder | Spring | 4 | 12 | Predicted | 17.6 |
| 6 | B | BCBC | Spring | 1 | 12 | Measured | 6.7 |
| 6 | B | BCBC | Spring | 1 | 12 | Predicted | 6.0 |
| 6 | B | BCBC | Spring | 2 | 12 | Measured | 9.9 |
| 6 | B | BCBC | Spring | 2 | 12 | Predicted | 8.9 |
| 6 | B | BCBC | Spring | 3 | 12 | Measured | 11.0 |
| 6 | B | BCBC | Spring | 3 | 12 | Predicted | 9.8 |
| 6 | B | BCBC | Spring | 4 | 12 | Measured | 16.8 |
| 6 | B | BCBC | Spring | 4 | 12 | Predicted | 15.1 |
| 7 | B | Wearing | Spring | 1 | 29 | Measured | 17.6 |
| 7 | B | Wearing | Spring | 1 | 29 | Predicted | 15.6 |
| 7 | B | Wearing | Spring | 2 | 29 | Measured | 8.3 |
| 7 | B | Wearing | Spring | 2 | 29 | Predicted | 7.4 |
| 7 | B | Wearing | Spring | 3 | 29 | Measured | 8.9 |
| 7 | B | Wearing | Spring | 3 | 29 | Predicted | 7.9 |
| 7 | B | Wearing | Spring | 4 | 29 | Measured | 31.0 |
| 7 | B | Wearing | Spring | 4 | 29 | Predicted | 27.6 |

| | | | | | | | |
|---|---|---|---|---|---|---|---|
| 7 | B | Binder | Spring | 1 | 29 | Measured | 8.7 |
| 7 | B | Binder | Spring | 1 | 29 | Predicted | 7.8 |
| 7 | B | Binder | Spring | 2 | 29 | Measured | 4.9 |
| 7 | B | Binder | Spring | 2 | 29 | Predicted | 4.4 |
| 7 | B | Binder | Spring | 3 | 29 | Measured | 5.0 |
| 7 | B | Binder | Spring | 3 | 29 | Predicted | 4.4 |
| 7 | B | Binder | Spring | 4 | 29 | Measured | 14.5 |
| 7 | B | Binder | Spring | 4 | 29 | Predicted | 13.0 |
| 7 | B | BCBC | Spring | 1 | 29 | Measured | 10.1 |
| 7 | B | BCBC | Spring | 1 | 29 | Predicted | 9.0 |
| 7 | B | BCBC | Spring | 2 | 29 | Measured | 4.5 |
| 7 | B | BCBC | Spring | 2 | 29 | Predicted | 4.0 |
| 7 | B | BCBC | Spring | 3 | 29 | Measured | 7.1 |
| 7 | B | BCBC | Spring | 3 | 29 | Predicted | 6.3 |
| 7 | B | BCBC | Spring | 4 | 29 | Measured | 14.4 |
| 7 | B | BCBC | Spring | 4 | 29 | Predicted | 12.9 |
| 8 | B | Wearing | Spring | 1 | 64 | Measured | 8.0 |
| 8 | B | Wearing | Spring | 1 | 64 | Predicted | 7.1 |
| 8 | B | Wearing | Spring | 2 | 64 | Measured | 4.4 |
| 8 | B | Wearing | Spring | 2 | 64 | Predicted | 3.9 |
| 8 | B | Wearing | Spring | 3 | 64 | Measured | 2.4 |
| 8 | B | Wearing | Spring | 3 | 64 | Predicted | 2.1 |
| 8 | B | Wearing | Spring | 4 | 64 | Measured | 14.2 |
| 8 | B | Wearing | Spring | 4 | 64 | Predicted | 12.6 |
| 8 | B | Binder | Spring | 1 | 64 | Measured | 6.0 |
| 8 | B | Binder | Spring | 1 | 64 | Predicted | 5.4 |
| 8 | B | Binder | Spring | 2 | 64 | Measured | 2.6 |
| 8 | B | Binder | Spring | 2 | 64 | Predicted | 2.3 |
| 8 | B | Binder | Spring | 3 | 64 | Measured | 2.2 |
| 8 | B | Binder | Spring | 3 | 64 | Predicted | 1.9 |
| 8 | B | Binder | Spring | 4 | 64 | Measured | 10.5 |

| | | | | | | | |
|---|---|---|---|---|---|---|---|
| 8 | B | Binder | Spring | 4 | 64 | Predicted | 9.4 |
| 8 | B | BCBC | Spring | 1 | 64 | Measured | 5.2 |
| 8 | B | BCBC | Spring | 1 | 64 | Predicted | 4.6 |
| 8 | B | BCBC | Spring | 2 | 64 | Measured | 7.4 |
| 8 | B | BCBC | Spring | 2 | 64 | Predicted | 6.6 |
| 8 | B | BCBC | Spring | 3 | 64 | Measured | 7.3 |
| 8 | B | BCBC | Spring | 3 | 64 | Predicted | 6.5 |
| 8 | B | BCBC | Spring | 4 | 64 | Measured | 13.9 |
| 8 | B | BCBC | Spring | 4 | 64 | Predicted | 12.4 |
| 9 | F | Wearing | Spring | 1 | 14 | Measured | 28.9 |
| 9 | F | Wearing | Spring | 1 | 14 | Predicted | 25.7 |
| 9 | F | Wearing | Spring | 2 | 14 | Measured | 21.3 |
| 9 | F | Wearing | Spring | 2 | 14 | Predicted | 18.9 |
| 9 | F | Wearing | Spring | 3 | 14 | Measured | 24.8 |
| 9 | F | Wearing | Spring | 3 | 14 | Predicted | 21.9 |
| 9 | F | Wearing | Spring | 4 | 14 | Measured | 27.2 |
| 9 | F | Wearing | Spring | 4 | 14 | Predicted | 24.2 |
| 9 | F | Binder | Spring | 1 | 14 | Measured | 18.3 |
| 9 | F | Binder | Spring | 1 | 14 | Predicted | 16.4 |
| 9 | F | Binder | Spring | 2 | 14 | Measured | 13.0 |
| 9 | F | Binder | Spring | 2 | 14 | Predicted | 11.6 |
| 9 | F | Binder | Spring | 3 | 14 | Measured | 14.3 |
| 9 | F | Binder | Spring | 3 | 14 | Predicted | 12.7 |
| 9 | F | Binder | Spring | 4 | 14 | Measured | 14.7 |
| 9 | F | Binder | Spring | 4 | 14 | Predicted | 13.2 |
| 9 | F | BCBC | Spring | 1 | 14 | Measured | 8.1 |
| 9 | F | BCBC | Spring | 1 | 14 | Predicted | 7.3 |
| 9 | F | BCBC | Spring | 2 | 14 | Measured | 19.5 |
| 9 | F | BCBC | Spring | 2 | 14 | Predicted | 17.5 |
| 9 | F | BCBC | Spring | 3 | 14 | Measured | 23.8 |
| 9 | F | BCBC | Spring | 3 | 14 | Predicted | 21.2 |

| | | | | | | | |
|---|---|---|---|---|---|---|---|
| 9 | F | BCBC | Spring | 4 | 14 | Measured | 20.7 |
| 9 | F | BCBC | Spring | 4 | 14 | Predicted | 18.5 |
| 10 | F | Wearing | Spring | 1 | 35 | Measured | 18.0 |
| 10 | F | Wearing | Spring | 1 | 35 | Predicted | 16.0 |
| 10 | F | Wearing | Spring | 2 | 35 | Measured | 11.4 |
| 10 | F | Wearing | Spring | 2 | 35 | Predicted | 10.1 |
| 10 | F | Wearing | Spring | 3 | 35 | Measured | 13.0 |
| 10 | F | Wearing | Spring | 3 | 35 | Predicted | 11.5 |
| 10 | F | Wearing | Spring | 4 | 35 | Measured | 15.2 |
| 10 | F | Wearing | Spring | 4 | 35 | Predicted | 13.5 |
| 10 | F | Binder | Spring | 1 | 35 | Measured | 10.5 |
| 10 | F | Binder | Spring | 1 | 35 | Predicted | 9.4 |
| 10 | F | Binder | Spring | 2 | 35 | Measured | 7.1 |
| 10 | F | Binder | Spring | 2 | 35 | Predicted | 6.3 |
| 10 | F | Binder | Spring | 3 | 35 | Measured | 9.0 |
| 10 | F | Binder | Spring | 3 | 35 | Predicted | 8.0 |
| 10 | F | Binder | Spring | 4 | 35 | Measured | 8.7 |
| 10 | F | Binder | Spring | 4 | 35 | Predicted | 7.8 |
| 10 | F | BCBC | Spring | 1 | 35 | Measured | 0.0 |
| 10 | F | BCBC | Spring | 1 | 35 | Predicted | 0.0 |
| 10 | F | BCBC | Spring | 2 | 35 | Measured | 14.1 |
| 10 | F | BCBC | Spring | 2 | 35 | Predicted | 12.6 |
| 10 | F | BCBC | Spring | 3 | 35 | Measured | 14.0 |
| 10 | F | BCBC | Spring | 3 | 35 | Predicted | 12.4 |
| 10 | F | BCBC | Spring | 4 | 35 | Measured | 10.6 |
| 10 | F | BCBC | Spring | 4 | 35 | Predicted | 9.5 |
| 11 | F | Wearing | Spring | 1 | 66 | Measured | 9.8 |
| 11 | F | Wearing | Spring | 1 | 66 | Predicted | 8.7 |
| 11 | F | Wearing | Spring | 2 | 66 | Measured | 5.3 |
| 11 | F | Wearing | Spring | 2 | 66 | Predicted | 4.7 |
| 11 | F | Wearing | Spring | 3 | 66 | Measured | 4.6 |

| | | | | | | | |
|---|---|---|---|---|---|---|---|
| 11 | F | Wearing | Spring | 3 | 66 | Predicted | 4.0 |
| 11 | F | Wearing | Spring | 4 | 66 | Measured | 8.7 |
| 11 | F | Wearing | Spring | 4 | 66 | Predicted | 7.7 |
| 11 | F | Binder | Spring | 1 | 66 | Measured | 9.7 |
| 11 | F | Binder | Spring | 1 | 66 | Predicted | 8.7 |
| 11 | F | Binder | Spring | 2 | 66 | Measured | 7.1 |
| 11 | F | Binder | Spring | 2 | 66 | Predicted | 6.3 |
| 11 | F | Binder | Spring | 3 | 66 | Measured | 6.2 |
| 11 | F | Binder | Spring | 3 | 66 | Predicted | 5.5 |
| 11 | F | Binder | Spring | 4 | 66 | Measured | 8.5 |
| 11 | F | Binder | Spring | 4 | 66 | Predicted | 7.6 |
| 11 | F | BCBC | Spring | 1 | 66 | Measured | 13.1 |
| 11 | F | BCBC | Spring | 1 | 66 | Predicted | 11.7 |
| 11 | F | BCBC | Spring | 2 | 66 | Measured | 13.7 |
| 11 | F | BCBC | Spring | 2 | 66 | Predicted | 12.2 |
| 11 | F | BCBC | Spring | 3 | 66 | Measured | 13.7 |
| 11 | F | BCBC | Spring | 3 | 66 | Predicted | 12.1 |
| 11 | F | BCBC | Spring | 4 | 66 | Measured | 11.1 |
| 11 | F | BCBC | Spring | 4 | 66 | Predicted | 9.9 |
| 12 | F | Binder | Summer | 1 | 7 | Measured | 118.8 |
| 12 | F | Binder | Summer | 1 | 7 | Predicted | 105.2 |
| 12 | F | Binder | Summer | 2 | 7 | Measured | 97.9 |
| 12 | F | Binder | Summer | 2 | 7 | Predicted | 86.7 |
| 12 | F | Binder | Summer | 3 | 7 | Measured | 101.7 |
| 12 | F | Binder | Summer | 3 | 7 | Predicted | 89.4 |
| 12 | F | Binder | Summer | 4 | 7 | Measured | 99.5 |
| 12 | F | Binder | Summer | 4 | 7 | Predicted | 88.1 |
| 12 | F | BCBC | Summer | 1 | 7 | Measured | 76.9 |
| 12 | F | BCBC | Summer | 1 | 7 | Predicted | 68.2 |
| 12 | F | BCBC | Summer | 2 | 7 | Measured | 60.7 |
| 12 | F | BCBC | Summer | 2 | 7 | Predicted | 53.8 |

| | | | | | | | |
|---|---|---|---|---|---|---|---|
| 12 | F | BCBC | Summer | 3 | 7 | Measured | 48.5 |
| 12 | F | BCBC | Summer | 3 | 7 | Predicted | 42.7 |
| 12 | F | BCBC | Summer | 4 | 7 | Measured | 55.1 |
| 12 | F | BCBC | Summer | 4 | 7 | Predicted | 48.9 |
| 13 | F | Binder | Summer | 1 | 67 | Measured | 21.8 |
| 13 | F | Binder | Summer | 1 | 67 | Predicted | 19.2 |
| 13 | F | Binder | Summer | 2 | 67 | Measured | 8.7 |
| 13 | F | Binder | Summer | 2 | 67 | Predicted | 7.7 |
| 13 | F | Binder | Summer | 3 | 67 | Measured | 16.1 |
| 13 | F | Binder | Summer | 3 | 67 | Predicted | 14.1 |
| 13 | F | Binder | Summer | 4 | 67 | Measured | 20.5 |
| 13 | F | Binder | Summer | 4 | 67 | Predicted | 18.1 |
| 13 | F | BCBC | Summer | 1 | 67 | Measured | 8.8 |
| 13 | F | BCBC | Summer | 1 | 67 | Predicted | 7.8 |
| 13 | F | BCBC | Summer | 2 | 67 | Measured | 9.9 |
| 13 | F | BCBC | Summer | 2 | 67 | Predicted | 8.7 |
| 13 | F | BCBC | Summer | 3 | 67 | Measured | 9.9 |
| 13 | F | BCBC | Summer | 3 | 67 | Predicted | 8.7 |
| 13 | F | BCBC | Summer | 4 | 67 | Measured | 15.4 |
| 13 | F | BCBC | Summer | 4 | 67 | Predicted | 13.6 |

**Table 2. Summary of measured and FE simulated vertical stresses for Blair.**

| Run# | Load Configuration | Location | Season | Axle | Actual Speed, kph | Data Source | Vertical Stress, kPa |
|---|---|---|---|---|---|---|---|
| 1 | B | Subbase | Spring | 1 | 42 | Measured | 12.9 |
| 1 | B | Subbase | Spring | 1 | 42 | Predicted | 14.7 |
| 1 | B | Subbase | Spring | 2 | 42 | Measured | 8.6 |
| 1 | B | Subbase | Spring | 2 | 42 | Predicted | 9.8 |
| 1 | B | Subbase | Spring | 3 | 42 | Measured | 8.9 |
| 1 | B | Subbase | Spring | 3 | 42 | Predicted | 10.1 |
| 1 | B | Subbase | Spring | 4 | 42 | Measured | 22.3 |
| 1 | B | Subbase | Spring | 4 | 42 | Predicted | 25.4 |
| 2 | B | Subbase | Summer | 1 | 61 | Measured | 12.2 |
| 2 | B | Subbase | Summer | 1 | 61 | Predicted | 14.0 |
| 2 | B | Subbase | Summer | 2 | 61 | Measured | 10.3 |
| 2 | B | Subbase | Summer | 2 | 61 | Predicted | 11.8 |
| 2 | B | Subbase | Summer | 3 | 61 | Measured | 9.2 |
| 2 | B | Subbase | Summer | 3 | 61 | Predicted | 10.5 |
| 2 | B | Subbase | Summer | 4 | 61 | Measured | 21.1 |
| 2 | B | Subbase | Summer | 4 | 61 | Predicted | 24.2 |
| 3 | F | Subbase | Summer | 1 | 39 | Measured | 17.4 |
| 3 | F | Subbase | Summer | 1 | 39 | Predicted | 19.9 |
| 3 | F | Subbase | Summer | 2 | 39 | Measured | 16.3 |
| 3 | F | Subbase | Summer | 2 | 39 | Predicted | 18.7 |
| 3 | F | Subbase | Summer | 3 | 39 | Measured | 15.9 |
| 3 | F | Subbase | Summer | 3 | 39 | Predicted | 18.2 |
| 3 | F | Subbase | Summer | 4 | 39 | Measured | 17.0 |
| 3 | F | Subbase | Summer | 4 | 39 | Predicted | 19.5 |
| 4 | B | Subbase | Fall | 1 | 35 | Measured | 7.8 |
| 4 | B | Subbase | Fall | 1 | 35 | Predicted | 8.9 |
| 4 | B | Subbase | Fall | 2 | 35 | Measured | 6.0 |
| 4 | B | Subbase | Fall | 2 | 35 | Predicted | 6.8 |

| | | | | | | | |
|---|---|---|---|---|---|---|---|
| 4 | B | Subbase | Fall | 3 | 35 | Measured | 5.3 |
| 4 | B | Subbase | Fall | 3 | 35 | Predicted | 6.0 |
| 4 | B | Subbase | Fall | 4 | 35 | Measured | 13.1 |
| 4 | B | Subbase | Fall | 4 | 35 | Predicted | 14.9 |
| 5 | B | Subbase | Fall | 1 | 68 | Measured | 6.3 |
| 5 | B | Subbase | Fall | 1 | 68 | Predicted | 7.1 |
| 5 | B | Subbase | Fall | 2 | 68 | Measured | 6.4 |
| 5 | B | Subbase | Fall | 2 | 68 | Predicted | 7.3 |
| 5 | B | Subbase | Fall | 3 | 68 | Measured | 5.9 |
| 5 | B | Subbase | Fall | 3 | 68 | Predicted | 6.7 |
| 5 | B | Subbase | Fall | 4 | 68 | Measured | 11.7 |
| 5 | B | Subbase | Fall | 4 | 68 | Predicted | 13.4 |
| 6 | B | Subgrade | Spring | 1 | 12 | Measured | 9.3 |
| 6 | B | Subgrade | Spring | 1 | 12 | Predicted | 10.6 |
| 6 | B | Subgrade | Spring | 2 | 12 | Measured | 6.3 |
| 6 | B | Subgrade | Spring | 2 | 12 | Predicted | 7.2 |
| 6 | B | Subgrade | Spring | 3 | 12 | Measured | 6.6 |
| 6 | B | Subgrade | Spring | 3 | 12 | Predicted | 7.5 |
| 6 | B | Subgrade | Spring | 4 | 12 | Measured | 14.9 |
| 6 | B | Subgrade | Spring | 4 | 12 | Predicted | 17.0 |
| 7 | B | Subgrade | Spring | 1 | 29 | Measured | 8.6 |
| 7 | B | Subgrade | Spring | 1 | 29 | Predicted | 9.8 |
| 7 | B | Subgrade | Spring | 2 | 29 | Measured | 6.6 |
| 7 | B | Subgrade | Spring | 2 | 29 | Predicted | 7.5 |
| 7 | B | Subgrade | Spring | 3 | 29 | Measured | 6.0 |
| 7 | B | Subgrade | Spring | 3 | 29 | Predicted | 6.8 |
| 7 | B | Subgrade | Spring | 4 | 29 | Measured | 13.2 |
| 7 | B | Subgrade | Spring | 4 | 29 | Predicted | 15.0 |
| 8 | B | Subgrade | Spring | 1 | 64 | Measured | 7.1 |
| 8 | B | Subgrade | Spring | 1 | 64 | Predicted | 8.1 |
| 8 | B | Subgrade | Spring | 2 | 64 | Measured | 6.9 |

| | | | | | | | |
|---|---|---|---|---|---|---|---|
| 8 | B | Subgrade | Spring | 2 | 64 | Predicted | 7.9 |
| 8 | B | Subgrade | Spring | 3 | 64 | Measured | 6.7 |
| 8 | B | Subgrade | Spring | 3 | 64 | Predicted | 7.6 |
| 8 | B | Subgrade | Spring | 4 | 64 | Measured | 14.0 |
| 8 | B | Subgrade | Spring | 4 | 64 | Predicted | 15.9 |
| 9 | F | Subbase | Spring | 1 | 14 | Measured | 10.7 |
| 9 | F | Subbase | Spring | 1 | 14 | Predicted | 12.2 |
| 9 | F | Subbase | Spring | 2 | 14 | Measured | 11.0 |
| 9 | F | Subbase | Spring | 2 | 14 | Predicted | 12.6 |
| 9 | F | Subbase | Spring | 3 | 14 | Measured | 11.8 |
| 9 | F | Subbase | Spring | 3 | 14 | Predicted | 13.5 |
| 9 | F | Subbase | Spring | 4 | 14 | Measured | 9.6 |
| 9 | F | Subbase | Spring | 4 | 14 | Predicted | 11.0 |
| 9 | F | Subgrade | Spring | 1 | 14 | Measured | 4.6 |
| 9 | F | Subgrade | Spring | 1 | 14 | Predicted | 5.2 |
| 9 | F | Subgrade | Spring | 2 | 14 | Measured | 1.7 |
| 9 | F | Subgrade | Spring | 2 | 14 | Predicted | 1.9 |
| 9 | F | Subgrade | Spring | 3 | 14 | Measured | 4.1 |
| 9 | F | Subgrade | Spring | 3 | 14 | Predicted | 4.7 |
| 9 | F | Subgrade | Spring | 4 | 14 | Measured | 0.4 |
| 9 | F | Subgrade | Spring | 4 | 14 | Predicted | 0.5 |
| 10 | F | Subbase | Spring | 1 | 35 | Measured | 10.1 |
| 10 | F | Subbase | Spring | 1 | 35 | Predicted | 11.5 |
| 10 | F | Subbase | Spring | 2 | 35 | Measured | 10.5 |
| 10 | F | Subbase | Spring | 2 | 35 | Predicted | 12.0 |
| 10 | F | Subbase | Spring | 3 | 35 | Measured | 11.4 |
| 10 | F | Subbase | Spring | 3 | 35 | Predicted | 13.0 |
| 10 | F | Subbase | Spring | 4 | 35 | Measured | 8.9 |
| 10 | F | Subbase | Spring | 4 | 35 | Predicted | 10.2 |
| 10 | F | Subgrade | Spring | 1 | 35 | Measured | 1.7 |
| 10 | F | Subgrade | Spring | 1 | 35 | Predicted | 1.9 |

| | | | | | | | |
|---|---|---|---|---|---|---|---|
| 10 | F | Subgrade | Spring | 2 | 35 | Measured | 0.6 |
| 10 | F | Subgrade | Spring | 2 | 35 | Predicted | 0.7 |
| 10 | F | Subgrade | Spring | 3 | 35 | Measured | 0.9 |
| 10 | F | Subgrade | Spring | 3 | 35 | Predicted | 1.0 |
| 10 | F | Subgrade | Spring | 4 | 35 | Measured | 0.2 |
| 10 | F | Subgrade | Spring | 4 | 35 | Predicted | 0.2 |
| 11 | F | Subbase | Spring | 1 | 66 | Measured | 7.9 |
| 11 | F | Subbase | Spring | 1 | 66 | Predicted | 9.0 |
| 11 | F | Subbase | Spring | 2 | 66 | Measured | 9.7 |
| 11 | F | Subbase | Spring | 2 | 66 | Predicted | 11.1 |
| 11 | F | Subbase | Spring | 3 | 66 | Measured | 9.9 |
| 11 | F | Subbase | Spring | 3 | 66 | Predicted | 11.3 |
| 11 | F | Subbase | Spring | 4 | 66 | Measured | 7.4 |
| 11 | F | Subbase | Spring | 4 | 66 | Predicted | 8.5 |
| 11 | F | Subgrade | Spring | 1 | 66 | Measured | 0.7 |
| 11 | F | Subgrade | Spring | 1 | 66 | Predicted | 0.8 |
| 11 | F | Subgrade | Spring | 2 | 66 | Measured | 0.6 |
| 11 | F | Subgrade | Spring | 2 | 66 | Predicted | 0.7 |
| 11 | F | Subgrade | Spring | 3 | 66 | Measured | 0.6 |
| 11 | F | Subgrade | Spring | 3 | 66 | Predicted | 0.7 |
| 12 | F | Subbase | Summer | 1 | 7 | Measured | 18.1 |
| 12 | F | Subbase | Summer | 1 | 7 | Predicted | 20.7 |
| 12 | F | Subbase | Summer | 2 | 7 | Measured | 16.3 |
| 12 | F | Subbase | Summer | 2 | 7 | Predicted | 18.7 |
| 12 | F | Subbase | Summer | 3 | 7 | Measured | 17.4 |
| 12 | F | Subbase | Summer | 3 | 7 | Predicted | 20.0 |
| 12 | F | Subbase | Summer | 4 | 7 | Measured | 14.1 |
| 12 | F | Subbase | Summer | 4 | 7 | Predicted | 16.2 |
| 13 | F | Subbase | Summer | 1 | 67 | Measured | 12.5 |
| 13 | F | Subbase | Summer | 1 | 67 | Predicted | 14.4 |
| 13 | F | Subbase | Summer | 2 | 67 | Measured | 15.0 |

| | | | | | | | |
|---|---|---|---|---|---|---|---|
| 13 | F | Subbase | Summer | 2 | 67 | Predicted | 17.2 |
| 13 | F | Subbase | Summer | 3 | 67 | Measured | 14.5 |
| 13 | F | Subbase | Summer | 3 | 67 | Predicted | 16.7 |
| 13 | F | Subbase | Summer | 4 | 67 | Measured | 12.9 |
| 13 | F | Subbase | Summer | 4 | 67 | Predicted | 14.8 |

**Table 3. Summary of measured and FE simulated horizontal strains for Warren.**

| Run# | Load Configuration | Location | Season | Axle | Actual Speed, kph | Data Source | Strain, E-6 |
|---|---|---|---|---|---|---|---|
| 1 | B | Binder | Summer | 1 | 68 | Measured | 20.3 |
| 1 | B | Binder | Summer | 1 | 68 | Predicted | 18.6 |
| 1 | B | Binder | Summer | 2 | 68 | Measured | 37.1 |
| 1 | B | Binder | Summer | 2 | 68 | Predicted | 34.0 |
| 1 | B | Binder | Summer | 3 | 68 | Measured | 39.9 |
| 1 | B | Binder | Summer | 3 | 68 | Predicted | 36.2 |
| 1 | B | Binder | Summer | 4 | 68 | Measured | 42.6 |
| 1 | B | Binder | Summer | 4 | 68 | Predicted | 39.0 |
| 2 | B | Binder | Summer | 1 | 100 | Measured | 16.9 |
| 2 | B | Binder | Summer | 1 | 100 | Predicted | 15.4 |
| 2 | B | Binder | Summer | 2 | 100 | Measured | 22.4 |
| 2 | B | Binder | Summer | 2 | 100 | Predicted | 20.5 |
| 2 | B | Binder | Summer | 3 | 100 | Measured | 27.3 |
| 2 | B | Binder | Summer | 3 | 100 | Predicted | 24.7 |
| 2 | B | Binder | Summer | 4 | 100 | Measured | 29.1 |
| 2 | B | Binder | Summer | 4 | 100 | Predicted | 26.6 |
| 3 | B | Binder | Summer | 1 | 36 | Measured | 23.3 |
| 3 | B | Binder | Summer | 1 | 36 | Predicted | 21.4 |
| 3 | B | Binder | Summer | 2 | 36 | Measured | 35.4 |
| 3 | B | Binder | Summer | 2 | 36 | Predicted | 32.6 |
| 3 | B | Binder | Summer | 3 | 36 | Measured | 41.1 |
| 3 | B | Binder | Summer | 3 | 36 | Predicted | 37.4 |
| 3 | B | Binder | Summer | 4 | 36 | Measured | 28.5 |
| 3 | B | Binder | Summer | 4 | 36 | Predicted | 26.2 |
| 4 | F | Binder | Summer | 1 | 35 | Measured | 8.7 |
| 4 | F | Binder | Summer | 1 | 35 | Predicted | 8.0 |
| 4 | F | BCBC | Summer | 1 | 35 | Measured | 5.6 |
| 4 | F | BCBC | Summer | 1 | 35 | Predicted | 5.1 |

| | | | | | | | |
|---|---|---|---|---|---|---|---|
| 4 | F | Binder | Summer | 2 | 35 | Measured | 16.2 |
| 4 | F | Binder | Summer | 2 | 35 | Predicted | 14.9 |
| 4 | F | BCBC | Summer | 2 | 35 | Measured | 5.5 |
| 4 | F | BCBC | Summer | 2 | 35 | Predicted | 5.0 |
| 4 | F | Binder | Summer | 3 | 35 | Measured | 16.2 |
| 4 | F | Binder | Summer | 3 | 35 | Predicted | 14.7 |
| 4 | F | BCBC | Summer | 3 | 35 | Measured | 5.2 |
| 4 | F | BCBC | Summer | 3 | 35 | Predicted | 4.7 |
| 4 | F | Binder | Summer | 4 | 35 | Measured | 10.3 |
| 4 | F | Binder | Summer | 4 | 35 | Predicted | 9.5 |
| 4 | F | BCBC | Summer | 4 | 35 | Measured | 4.0 |
| 4 | F | BCBC | Summer | 4 | 35 | Predicted | 3.7 |
| 5 | F | Binder | Summer | 1 | 68 | Measured | 7.9 |
| 5 | F | Binder | Summer | 1 | 68 | Predicted | 7.3 |
| 5 | F | BCBC | Summer | 1 | 68 | Measured | 3.4 |
| 5 | F | BCBC | Summer | 1 | 68 | Predicted | 3.1 |
| 5 | F | Binder | Summer | 2 | 68 | Measured | 13.6 |
| 5 | F | Binder | Summer | 2 | 68 | Predicted | 12.5 |
| 5 | F | BCBC | Summer | 2 | 68 | Measured | 4.3 |
| 5 | F | BCBC | Summer | 2 | 68 | Predicted | 4.0 |
| 5 | F | BCBC | Summer | 3 | 68 | Measured | 3.9 |
| 5 | F | BCBC | Summer | 3 | 68 | Predicted | 3.5 |
| 5 | F | Binder | Summer | 4 | 68 | Measured | 9.6 |
| 5 | F | Binder | Summer | 4 | 68 | Predicted | 8.8 |
| 5 | F | BCBC | Summer | 4 | 68 | Measured | 3.2 |
| 5 | F | BCBC | Summer | 4 | 68 | Predicted | 3.0 |
| 6 | F | Binder | Summer | 1 | 101 | Measured | 6.8 |
| 6 | F | Binder | Summer | 1 | 101 | Predicted | 6.2 |
| 6 | F | BCBC | Summer | 1 | 101 | Measured | 2.9 |
| 6 | F | BCBC | Summer | 1 | 101 | Predicted | 2.7 |
| 6 | F | Binder | Summer | 2 | 101 | Measured | 12.6 |

| | | | | | | | |
|---|---|---|---|---|---|---|---|
| 6 | F | Binder | Summer | 2 | 101 | Predicted | 11.5 |
| 6 | F | BCBC | Summer | 2 | 101 | Measured | 3.3 |
| 6 | F | BCBC | Summer | 2 | 101 | Predicted | 3.0 |
| 6 | F | Binder | Summer | 3 | 101 | Measured | 12.6 |
| 6 | F | Binder | Summer | 3 | 101 | Predicted | 11.4 |
| 6 | F | BCBC | Summer | 3 | 101 | Measured | 3.3 |
| 6 | F | BCBC | Summer | 3 | 101 | Predicted | 3.0 |
| 6 | F | Binder | Summer | 4 | 101 | Measured | 7.5 |
| 6 | F | Binder | Summer | 4 | 101 | Predicted | 6.9 |
| 6 | F | BCBC | Summer | 4 | 101 | Measured | 1.8 |
| 6 | F | BCBC | Summer | 4 | 101 | Predicted | 1.6 |
| 7 | B | Binder | Summer | 1 | 38 | Measured | 15.9 |
| 7 | B | Binder | Summer | 1 | 38 | Predicted | 14.6 |
| 7 | B | BCBC | Summer | 1 | 38 | Measured | 4.2 |
| 7 | B | BCBC | Summer | 1 | 38 | Predicted | 3.9 |
| 7 | B | Binder | Summer | 2 | 38 | Measured | 11.3 |
| 7 | B | Binder | Summer | 2 | 38 | Predicted | 10.4 |
| 7 | B | BCBC | Summer | 2 | 38 | Measured | 3.6 |
| 7 | B | BCBC | Summer | 2 | 38 | Predicted | 3.3 |
| 7 | B | Binder | Summer | 3 | 38 | Measured | 11.3 |
| 7 | B | Binder | Summer | 3 | 38 | Predicted | 10.3 |
| 7 | B | BCBC | Summer | 3 | 38 | Measured | 3.1 |
| 7 | B | BCBC | Summer | 3 | 38 | Predicted | 2.8 |
| 7 | B | Binder | Summer | 4 | 38 | Measured | 24.2 |
| 7 | B | Binder | Summer | 4 | 38 | Predicted | 22.2 |
| 7 | B | BCBC | Summer | 4 | 38 | Measured | 8.1 |
| 7 | B | BCBC | Summer | 4 | 38 | Predicted | 7.4 |
| 8 | B | Binder | Summer | 1 | 69 | Measured | 12.6 |
| 8 | B | Binder | Summer | 1 | 69 | Predicted | 11.6 |
| 8 | B | BCBC | Summer | 1 | 69 | Measured | 4.2 |
| 8 | B | BCBC | Summer | 1 | 69 | Predicted | 3.9 |

| | | | | | | | |
|---|---|---|---|---|---|---|---|
| 8 | B | Binder | Summer | 2 | 69 | Measured | 11.9 |
| 8 | B | Binder | Summer | 2 | 69 | Predicted | 10.9 |
| 8 | B | BCBC | Summer | 2 | 69 | Measured | 2.1 |
| 8 | B | BCBC | Summer | 2 | 69 | Predicted | 1.9 |
| 8 | B | Binder | Summer | 3 | 69 | Measured | 11.9 |
| 8 | B | Binder | Summer | 3 | 69 | Predicted | 10.8 |
| 8 | B | BCBC | Summer | 3 | 69 | Measured | 2.0 |
| 8 | B | BCBC | Summer | 3 | 69 | Predicted | 1.8 |
| 8 | B | Binder | Summer | 4 | 69 | Measured | 20.4 |
| 8 | B | Binder | Summer | 4 | 69 | Predicted | 18.7 |
| 8 | B | BCBC | Summer | 4 | 69 | Measured | 3.8 |
| 8 | B | BCBC | Summer | 4 | 69 | Predicted | 3.5 |
| 9 | B | Binder | Summer | 1 | 99 | Measured | 9.0 |
| 9 | B | Binder | Summer | 1 | 99 | Predicted | 8.2 |
| 9 | B | BCBC | Summer | 1 | 99 | Measured | 3.4 |
| 9 | B | BCBC | Summer | 1 | 99 | Predicted | 3.1 |
| 9 | B | Binder | Summer | 2 | 99 | Measured | 10.8 |
| 9 | B | Binder | Summer | 2 | 99 | Predicted | 9.9 |
| 9 | B | BCBC | Summer | 2 | 99 | Measured | 2.7 |
| 9 | B | BCBC | Summer | 2 | 99 | Predicted | 2.5 |
| 9 | B | Binder | Summer | 3 | 99 | Measured | 10.8 |
| 9 | B | Binder | Summer | 3 | 99 | Predicted | 9.8 |
| 9 | B | BCBC | Summer | 3 | 99 | Measured | 2.7 |
| 9 | B | BCBC | Summer | 3 | 99 | Predicted | 2.4 |
| 9 | B | Binder | Summer | 4 | 99 | Measured | 17.7 |
| 9 | B | Binder | Summer | 4 | 99 | Predicted | 16.2 |
| 9 | B | BCBC | Summer | 4 | 99 | Measured | 3.8 |
| 9 | B | BCBC | Summer | 4 | 99 | Predicted | 3.5 |
| 10 | F | Binder | Fall | 1 | 36 | Measured | 6.4 |
| 10 | F | Binder | Fall | 1 | 36 | Predicted | 5.9 |
| 10 | F | BCBC | Fall | 1 | 36 | Measured | 5.4 |

| | | | | | | | |
|---|---|---|---|---|---|---|---|
| 10 | F | BCBC | Fall | 1 | 36 | Predicted | 5.0 |
| 10 | F | Binder | Fall | 2 | 36 | Measured | 8.3 |
| 10 | F | Binder | Fall | 2 | 36 | Predicted | 7.7 |
| 10 | F | BCBC | Fall | 2 | 36 | Measured | 6.1 |
| 10 | F | BCBC | Fall | 2 | 36 | Predicted | 5.7 |
| 10 | F | Binder | Fall | 3 | 36 | Measured | 7.6 |
| 10 | F | Binder | Fall | 3 | 36 | Predicted | 7.0 |
| 10 | F | BCBC | Fall | 3 | 36 | Measured | 5.9 |
| 10 | F | BCBC | Fall | 3 | 36 | Predicted | 5.4 |
| 10 | F | Binder | Fall | 4 | 36 | Measured | 6.7 |
| 10 | F | Binder | Fall | 4 | 36 | Predicted | 6.2 |
| 10 | F | BCBC | Fall | 4 | 36 | Measured | 5.7 |
| 10 | F | BCBC | Fall | 4 | 36 | Predicted | 5.3 |
| 11 | F | Binder | Fall | 1 | 71 | Measured | 5.0 |
| 11 | F | Binder | Fall | 1 | 71 | Predicted | 4.6 |
| 11 | F | BCBC | Fall | 1 | 71 | Measured | 3.8 |
| 11 | F | BCBC | Fall | 1 | 71 | Predicted | 3.5 |
| 11 | F | Binder | Fall | 2 | 71 | Measured | 7.1 |
| 11 | F | Binder | Fall | 2 | 71 | Predicted | 6.6 |
| 11 | F | BCBC | Fall | 2 | 71 | Measured | 4.8 |
| 11 | F | BCBC | Fall | 2 | 71 | Predicted | 4.5 |
| 11 | F | Binder | Fall | 3 | 71 | Measured | 7.1 |
| 11 | F | Binder | Fall | 3 | 71 | Predicted | 6.5 |
| 11 | F | BCBC | Fall | 3 | 71 | Measured | 4.6 |
| 11 | F | BCBC | Fall | 3 | 71 | Predicted | 4.2 |
| 11 | F | Binder | Fall | 4 | 71 | Measured | 5.1 |
| 11 | F | Binder | Fall | 4 | 71 | Predicted | 4.7 |
| 11 | F | BCBC | Fall | 4 | 71 | Measured | 3.9 |
| 11 | F | BCBC | Fall | 4 | 71 | Predicted | 3.6 |
| 12 | F | Binder | Fall | 1 | 96 | Measured | 3.6 |
| 12 | F | Binder | Fall | 1 | 96 | Predicted | 3.3 |

| | | | | | | | |
|---|---|---|---|---|---|---|---|
| 12 | F | BCBC | Fall | 1 | 96 | Measured | 2.5 |
| 12 | F | BCBC | Fall | 1 | 96 | Predicted | 2.3 |
| 12 | F | Binder | Fall | 2 | 96 | Measured | 6.7 |
| 12 | F | Binder | Fall | 2 | 96 | Predicted | 6.2 |
| 12 | F | BCBC | Fall | 2 | 96 | Measured | 4.8 |
| 12 | F | BCBC | Fall | 2 | 96 | Predicted | 4.4 |
| 12 | F | Binder | Fall | 3 | 96 | Measured | 6.7 |
| 12 | F | Binder | Fall | 3 | 96 | Predicted | 6.1 |
| 12 | F | BCBC | Fall | 3 | 96 | Measured | 4.7 |
| 12 | F | BCBC | Fall | 3 | 96 | Predicted | 4.3 |
| 12 | F | Binder | Fall | 4 | 96 | Measured | 4.4 |
| 12 | F | Binder | Fall | 4 | 96 | Predicted | 4.1 |
| 12 | F | BCBC | Fall | 4 | 96 | Measured | 3.2 |
| 12 | F | BCBC | Fall | 4 | 96 | Predicted | 2.9 |
| 13 | B | BCBC | Fall | 1 | 11 | Measured | 5.0 |
| 13 | B | BCBC | Fall | 1 | 11 | Predicted | 4.6 |
| 13 | B | Binder | Fall | 2 | 11 | Measured | 10.9 |
| 13 | B | Binder | Fall | 2 | 11 | Predicted | 10.1 |
| 13 | B | BCBC | Fall | 2 | 11 | Measured | 5.1 |
| 13 | B | BCBC | Fall | 2 | 11 | Predicted | 4.7 |
| 13 | B | Binder | Fall | 3 | 11 | Measured | 9.9 |
| 13 | B | Binder | Fall | 3 | 11 | Predicted | 9.1 |
| 13 | B | BCBC | Fall | 3 | 11 | Measured | 4.8 |
| 13 | B | BCBC | Fall | 3 | 11 | Predicted | 4.4 |
| 13 | B | Binder | Fall | 4 | 11 | Measured | 19.1 |
| 13 | B | Binder | Fall | 4 | 11 | Predicted | 17.7 |
| 13 | B | BCBC | Fall | 4 | 11 | Measured | 11.1 |
| 13 | B | BCBC | Fall | 4 | 11 | Predicted | 10.3 |
| 14 | B | Binder | Fall | 1 | 39 | Measured | 7.5 |
| 14 | B | Binder | Fall | 1 | 39 | Predicted | 7.0 |
| 14 | B | BCBC | Fall | 1 | 39 | Measured | 4.2 |

| | | | | | | | |
|---|---|---|---|---|---|---|---|
| 14 | B | BCBC | Fall | 1 | 39 | Predicted | 3.9 |
| 14 | B | Binder | Fall | 2 | 39 | Measured | 4.8 |
| 14 | B | Binder | Fall | 2 | 39 | Predicted | 4.5 |
| 14 | B | BCBC | Fall | 2 | 39 | Measured | 3.6 |
| 14 | B | BCBC | Fall | 2 | 39 | Predicted | 3.4 |
| 14 | B | Binder | Fall | 3 | 39 | Measured | 5.2 |
| 14 | B | Binder | Fall | 3 | 39 | Predicted | 4.8 |
| 14 | B | BCBC | Fall | 3 | 39 | Measured | 3.3 |
| 14 | B | BCBC | Fall | 3 | 39 | Predicted | 3.1 |
| 14 | B | Binder | Fall | 4 | 39 | Measured | 12.4 |
| 14 | B | Binder | Fall | 4 | 39 | Predicted | 11.5 |
| 14 | B | BCBC | Fall | 4 | 39 | Measured | 8.1 |
| 14 | B | BCBC | Fall | 4 | 39 | Predicted | 7.5 |
| 15 | B | Binder | Fall | 1 | 65 | Measured | 6.5 |
| 15 | B | Binder | Fall | 1 | 65 | Predicted | 6.0 |
| 15 | B | BCBC | Fall | 1 | 65 | Measured | 4.0 |
| 15 | B | BCBC | Fall | 1 | 65 | Predicted | 3.7 |
| 15 | B | Binder | Fall | 2 | 65 | Measured | 4.9 |
| 15 | B | Binder | Fall | 2 | 65 | Predicted | 4.5 |
| 15 | B | BCBC | Fall | 2 | 65 | Measured | 2.4 |
| 15 | B | BCBC | Fall | 2 | 65 | Predicted | 2.2 |
| 15 | B | Binder | Fall | 3 | 65 | Measured | 4.9 |
| 15 | B | Binder | Fall | 3 | 65 | Predicted | 4.5 |
| 15 | B | BCBC | Fall | 3 | 65 | Measured | 2.8 |
| 15 | B | BCBC | Fall | 3 | 65 | Predicted | 2.6 |
| 15 | B | Binder | Fall | 4 | 65 | Measured | 9.6 |
| 15 | B | Binder | Fall | 4 | 65 | Predicted | 8.9 |
| 15 | B | BCBC | Fall | 4 | 65 | Measured | 5.7 |
| 15 | B | BCBC | Fall | 4 | 65 | Predicted | 5.3 |
| 16 | B | Binder | Fall | 1 | 98 | Measured | 4.4 |
| 16 | B | Binder | Fall | 1 | 98 | Predicted | 4.1 |

| | | | | | | | |
|---|---|---|---|---|---|---|---|
| 16 | B | BCBC | Fall | 1 | 98 | Measured | 2.1 |
| 16 | B | BCBC | Fall | 1 | 98 | Predicted | 1.9 |
| 16 | B | Binder | Fall | 2 | 98 | Measured | 4.2 |
| 16 | B | Binder | Fall | 2 | 98 | Predicted | 3.9 |
| 16 | B | BCBC | Fall | 2 | 98 | Measured | 3.1 |
| 16 | B | BCBC | Fall | 2 | 98 | Predicted | 2.9 |
| 16 | B | Binder | Fall | 3 | 98 | Measured | 4.2 |
| 16 | B | Binder | Fall | 3 | 98 | Predicted | 3.8 |
| 16 | B | BCBC | Fall | 3 | 98 | Measured | 3.1 |
| 16 | B | BCBC | Fall | 3 | 98 | Predicted | 2.9 |
| 16 | B | Binder | Fall | 4 | 98 | Measured | 7.0 |
| 16 | B | Binder | Fall | 4 | 98 | Predicted | 6.5 |
| 16 | B | BCBC | Fall | 4 | 98 | Measured | 4.7 |
| 16 | B | BCBC | Fall | 4 | 98 | Predicted | 4.3 |
| 17 | F | Binder | Spring | 1 | 33 | Measured | 8.4 |
| 17 | F | Binder | Spring | 1 | 33 | Predicted | 7.8 |
| 17 | F | BCBC | Spring | 1 | 33 | Measured | 4.2 |
| 17 | F | BCBC | Spring | 1 | 33 | Predicted | 3.9 |
| 17 | F | Binder | Spring | 2 | 33 | Measured | 9.1 |
| 17 | F | Binder | Spring | 2 | 33 | Predicted | 8.4 |
| 17 | F | BCBC | Spring | 2 | 33 | Measured | 4.3 |
| 17 | F | BCBC | Spring | 2 | 33 | Predicted | 4.0 |
| 17 | F | Binder | Spring | 3 | 33 | Measured | 8.5 |
| 17 | F | Binder | Spring | 3 | 33 | Predicted | 7.8 |
| 17 | F | BCBC | Spring | 3 | 33 | Measured | 3.8 |
| 17 | F | BCBC | Spring | 3 | 33 | Predicted | 3.5 |
| 17 | F | Binder | Spring | 4 | 33 | Measured | 7.6 |
| 17 | F | Binder | Spring | 4 | 33 | Predicted | 7.0 |
| 17 | F | BCBC | Spring | 4 | 33 | Measured | 3.5 |
| 17 | F | BCBC | Spring | 4 | 33 | Predicted | 3.2 |
| 18 | F | Binder | Spring | 1 | 66 | Measured | 5.5 |

| | | | | | | | |
|---|---|---|---|---|---|---|---|
| 18 | F | Binder | Spring | 1 | 66 | Predicted | 5.1 |
| 18 | F | BCBC | Spring | 1 | 66 | Measured | 2.7 |
| 18 | F | BCBC | Spring | 1 | 66 | Predicted | 2.5 |
| 18 | F | Binder | Spring | 2 | 66 | Measured | 7.0 |
| 18 | F | Binder | Spring | 2 | 66 | Predicted | 6.5 |
| 18 | F | BCBC | Spring | 2 | 66 | Measured | 3.0 |
| 18 | F | BCBC | Spring | 2 | 66 | Predicted | 2.8 |
| 18 | F | Binder | Spring | 3 | 66 | Measured | 6.5 |
| 18 | F | Binder | Spring | 3 | 66 | Predicted | 6.0 |
| 18 | F | BCBC | Spring | 3 | 66 | Measured | 2.6 |
| 18 | F | BCBC | Spring | 3 | 66 | Predicted | 2.4 |
| 18 | F | Binder | Spring | 4 | 66 | Measured | 5.2 |
| 18 | F | Binder | Spring | 4 | 66 | Predicted | 4.8 |
| 18 | F | BCBC | Spring | 4 | 66 | Measured | 2.2 |
| 18 | F | BCBC | Spring | 4 | 66 | Predicted | 2.0 |
| 19 | F | Binder | Spring | 1 | 100 | Measured | 3.8 |
| 19 | F | Binder | Spring | 1 | 100 | Predicted | 3.5 |
| 19 | F | BCBC | Spring | 1 | 100 | Measured | 2.3 |
| 19 | F | BCBC | Spring | 1 | 100 | Predicted | 2.1 |
| 19 | F | Binder | Spring | 2 | 100 | Measured | 7.4 |
| 19 | F | Binder | Spring | 2 | 100 | Predicted | 6.8 |
| 19 | F | BCBC | Spring | 2 | 100 | Measured | 2.5 |
| 19 | F | BCBC | Spring | 2 | 100 | Predicted | 2.3 |
| 19 | F | Binder | Spring | 3 | 100 | Measured | 7.4 |
| 19 | F | Binder | Spring | 3 | 100 | Predicted | 6.8 |
| 19 | F | BCBC | Spring | 3 | 100 | Measured | 2.5 |
| 19 | F | BCBC | Spring | 3 | 100 | Predicted | 2.3 |
| 19 | F | Binder | Spring | 4 | 100 | Measured | 5.1 |
| 19 | F | Binder | Spring | 4 | 100 | Predicted | 4.7 |
| 19 | F | BCBC | Spring | 4 | 100 | Measured | 1.7 |
| 19 | F | BCBC | Spring | 4 | 100 | Predicted | 1.5 |

| | | | | | | | |
|---|---|---|---|---|---|---|---|
| 20 | B | Binder | Spring | 1 | 34 | Measured | 8.3 |
| 20 | B | Binder | Spring | 1 | 34 | Predicted | 7.7 |
| 20 | B | BCBC | Spring | 1 | 34 | Measured | 3.5 |
| 20 | B | BCBC | Spring | 1 | 34 | Predicted | 3.3 |
| 20 | B | Binder | Spring | 2 | 34 | Measured | 6.4 |
| 20 | B | Binder | Spring | 2 | 34 | Predicted | 5.9 |
| 20 | B | BCBC | Spring | 2 | 34 | Measured | 2.5 |
| 20 | B | BCBC | Spring | 2 | 34 | Predicted | 2.3 |
| 20 | B | Binder | Spring | 3 | 34 | Measured | 6.1 |
| 20 | B | Binder | Spring | 3 | 34 | Predicted | 5.6 |
| 20 | B | BCBC | Spring | 3 | 34 | Measured | 2.1 |
| 20 | B | BCBC | Spring | 3 | 34 | Predicted | 1.9 |
| 20 | B | Binder | Spring | 4 | 34 | Measured | 15.8 |
| 20 | B | Binder | Spring | 4 | 34 | Predicted | 14.6 |
| 20 | B | BCBC | Spring | 4 | 34 | Measured | 5.7 |
| 20 | B | BCBC | Spring | 4 | 34 | Predicted | 5.3 |
| 21 | B | Binder | Spring | 1 | 68 | Measured | 6.2 |
| 21 | B | Binder | Spring | 1 | 68 | Predicted | 5.7 |
| 21 | B | BCBC | Spring | 1 | 68 | Measured | 2.3 |
| 21 | B | BCBC | Spring | 1 | 68 | Predicted | 2.1 |
| 21 | B | Binder | Spring | 2 | 68 | Measured | 5.7 |
| 21 | B | Binder | Spring | 2 | 68 | Predicted | 5.3 |
| 21 | B | BCBC | Spring | 2 | 68 | Measured | 1.7 |
| 21 | B | BCBC | Spring | 2 | 68 | Predicted | 1.6 |
| 21 | B | Binder | Spring | 3 | 68 | Measured | 5.7 |
| 21 | B | Binder | Spring | 3 | 68 | Predicted | 5.2 |
| 21 | B | BCBC | Spring | 3 | 68 | Measured | 1.6 |
| 21 | B | BCBC | Spring | 3 | 68 | Predicted | 1.5 |
| 21 | B | Binder | Spring | 4 | 68 | Measured | 10.5 |
| 21 | B | Binder | Spring | 4 | 68 | Predicted | 9.7 |
| 21 | B | BCBC | Spring | 4 | 68 | Measured | 4.2 |

| | | | | | | | |
|---|---|---|---|---|---|---|---|
| 21 | B | BCBC | Spring | 4 | 68 | Predicted | 3.9 |
| 22 | B | Binder | Spring | 1 | 96 | Measured | 4.7 |
| 22 | B | Binder | Spring | 1 | 96 | Predicted | 4.3 |
| 22 | B | BCBC | Spring | 1 | 96 | Measured | 1.3 |
| 22 | B | BCBC | Spring | 1 | 96 | Predicted | 1.2 |
| 22 | B | Binder | Spring | 2 | 96 | Measured | 5.3 |
| 22 | B | Binder | Spring | 2 | 96 | Predicted | 4.9 |
| 22 | B | BCBC | Spring | 2 | 96 | Measured | 1.7 |
| 22 | B | BCBC | Spring | 2 | 96 | Predicted | 1.5 |
| 22 | B | Binder | Spring | 3 | 96 | Measured | 5.3 |
| 22 | B | Binder | Spring | 3 | 96 | Predicted | 4.8 |
| 22 | B | BCBC | Spring | 3 | 96 | Measured | 1.6 |
| 22 | B | BCBC | Spring | 3 | 96 | Predicted | 1.4 |
| 22 | B | Binder | Spring | 4 | 96 | Measured | 8.9 |
| 22 | B | Binder | Spring | 4 | 96 | Predicted | 8.2 |
| 22 | B | BCBC | Spring | 4 | 96 | Measured | 3.4 |
| 22 | B | BCBC | Spring | 4 | 96 | Predicted | 3.2 |